NMR probing of the polymer structure in UV curable acrylate coatings

Küchel, J.

Award date:
2006

NMR probing of the polymer structure in UV curable acrylate coatings

MRL/TPM 2006-01

Master thesis
Jan Küchel
November 2004-February 2006
TPM-2006-01

Supervisors:
Ir. S.J.F. Erich
Dr. ir. H.P. Huinink
Prof. dr. ir. K. Kopinga

TU/e technische universiteit eindhoven

Eindhoven University of Technology
Faculty of Applied Physics

NMR probing of the polymer structure in UV curable acrylate coatings

Master thesis
Jan Küchel
November 2004-February 2006
TPM-2006-01

Supervisors:
Ir. S.J.F. Erich
Dr. ir. H.P. Huinink
Prof. dr. ir. K. Kopinga

TU/e technische universiteit eindhoven

Eindhoven University of Technology
Faculty of Applied Physics

Abstract

Ultra violet (UV) curable acrylates are a class of coatings, which are more and more used. Their importance increases due to more stringent environmental regulations, concerning the use of volatile organic compounds (VOC) in coatings. Upon exposure to UV radiation, the acrylate molecules polymerise, forming a solid coating. This process is called curing. More fundamental knowledge is required about the factors that influence the final polymer structure, like the duration of exposure to UV radiation, or the types of chemicals. Absorption and scattering of UV radiation, but also oxygen inhibition, can have a depth dependent influence on the final polymer structure. Many of the current techniques which can provide knowledge of the polymer structure are either limited to optically transparant coatings or are unable to provide depth resolved information. High spatial resolution Nuclear Magnetic Resonance (NMR) is a technique which can in principle investigate the polymer structure as a function of depth, even in non-transparant coatings.

In this study NMR measurements on two types of model systems of UV cured acrylates are presented: UV cured 2-ethyl hexyl acrylate (EHA) and UV cured poly(ethylene glycol)diacrylate (PEGDA).

EHA forms branched chains upon curing. A thermal activation with a characteristic energy barrier of $(4.7 \pm 0.3) \times 10^{-20}$ J of the motions of the polymer is observed.

PEGDA forms a cross-linked polymer network upon curing, of which the glass transition temperature T_g can be varied. A linear relation between the transverse relaxation time T_2 and the glass transition temperature T_g is experimentally confirmed.

Experiments on a triple layer poly-urethane demonstrate the possibility to obtain depth resolved information on T_g.

Contents

Chapter 1

Introduction and motivation

1.1 Why coatings?

A coating is a thin continuous layer applied to a surface. Purposes for coatings can include energy savings, corrosion prevention, hygienics (e.g. easy cleaning and fungal resistance), impact and abrasion resistance and decoration.
The economic advantages of coatings are huge. For example, ships can save 40% fuel because of drag-reducing coatings, saving 7.2 million tons of fuel annually for the whole world fleet[1]. A steel sea bridge without protective coating would suffer severe corrosion within a few years. A coating, costing generally several hundred times less than the bridge, can protect it for up to 15–25 years, reducing the need for maintenance and increasing the lifetime. In the same way a wooden structure can be protected from moisture and rotting. There are numerous similar examples where the lifetime is increased and maintenance costs are dramatically reduced by a coating of marginal cost. Coatings with only a decorative or esthetic function can offer added value by increasing the attractiveness of a product. Coatings can also offer the possibility of material substitution. For example, coated steel can perform many tasks which otherwise would require much more expensive metals or alloys.

1.2 Composition and types of coatings

A coating before application (paint) consists of a binder and often a diluent or solvent and additives. The binder is the part that eventually solidifies and creates the final film. Typical binders are acrylics, polyesters, and latexes.
The solvent or diluent is used to adjust the viscosity of the paint, making application possible or easier. Typical examples are water and hydrocarbons. The solvents or diluents evaporate after application of the coating.
The additives affect the application, the solidification process, or the properties after curing. Additives include catalysts affecting chemical processes, dyes for colouration, and chemical stabilisers increasing the durability.
After application the coating solidifies: the solvents or diluents evaporate and a curing reaction takes place. The processes responsible for curing include poly-

merisation, oxidation, cooling or a combination of these.
The rate of solidification depends on the curing of the binder as well as on the evaporation of the diluent or solvent. Volatile diluents or solvents often provide a fast rate of evaporation but are often harmful for the environment. Because of more stringent environmental issues and health regulations there is an increasing interest in coatings without these volatile organical compounds (VOC). Waterborne coatings do not contain harmful solvents but generally have the disadvantage of a lower curing rate. Coatings which harden on cooling, such as enamel do not contain harmful solvents, but the coating and the material underneath the coating have to be heated to high temperatures. This limits the latter type of coating to materials and products with high melting points.
A group of coatings without VOC but with a fast curing reaction near room temperature are UV curable coatings.

1.3 UV curable coatings

UV curable coatings cure under the influence of ultra violet (UV) radiation. Typical ingredients for an UV curable coating are multifunctional oligomers, reactive diluents or monomers, photoinitiators to start the curing reaction and inhibitors to prevent spontaneous curing. The curing reaction is initiated by the absorption of UV light by a photoinitiator and is followed by free-radical polymerisation of the oligomers.

Advantages and disadvantages Besides the advantage of low or zero VOC emission, UV curable coatings can also offer very short curing times of a few seconds, increasing the efficiency of industrial processes. The potentially very high degree of cross-linking of the polymers improves the scratch-resistance[2].
Problems in the application of UV curable coatings include toxicity of the resins and 'line-of-sight' curing: the curing process is limited to areas accessible to UV radiation. This limits the possibilities for the curing of highly pigmented or metallic coatings. Moreover, in very hard and densely cross-linked products the mobility of the reactive substances is reduced during hardening, which results in the presence of unreacted residues which dramatically reduce the weathering resistance[3].

Investigation of the degree of curing The degree of cross-linking (the ratio between the number of actually formed cross-links and the number of theoretically possible cross-links) depends on many variables, like the duration of exposure to UV radiation, as well as the intensity and wavelength of the UV-light source. The chemical variables influencing the degree of cross-linking include the photoinitiator, the mobility of the reacting substances, and the possible presence of other reacting substances like oxygen. To optimise the duration and energy consumption of the curing process, it is necessary to have information on the degree of cross-linking in the coating.
Several techniques suitable for the investigation of the degree of cross-linking can

be distinguished: some techniques are optical, others non-optical, and some techniques provide depth-resolved information. Some examples are Raman- and IR-spectroscopy and the similar technique of confocal Raman microscopy. These are optical techniques, of which only confocal Raman microscopy provides depth resolved information. Non-optical techniques include differential scanning calorimetry (DSC), thermo mechanical analysis (TMA), and micro-indentation, which are all non-depth-resolving.
Depth-resolved information on the degree of cross-linking is especially important in non-transparent coatings, because the incident UV radiation is absorbed and scattered by e.g. colouring pigments. This can lead to inhomogeneous curing. Unfortunately, the use of optical techniques is limited to optically transparent coatings, while traditional non-optical techniques lack the possibility of depth-resolved information. This creates the need for a depth-resolving technique which is suitable for non-transparent coatings.

High spatial resolution NMR A possible technique satisfying these requirements is very high spatial resolution nuclear magnetic resonance (NMR) imaging, if it is possible to get information on the polymer structure from the NMR signal. Litvinov and Dias[4] have shown that it is possible to get information on the properties of a polymer structure from the NMR signal. In their research the NMR measurements were performed without spatial resolution. If the same type of measurements can be performed in NMR setups with a high (order of micrometres) resolution, this would mean a new and suitable way to investigate the network structure even in non-transparent coatings.

1.4 Outline of this report

In chapter 2 the basics of NMR and one dimensional (1D) NMR imaging are discussed, as well as the NMR pulse sequences relevant for this report. Next, the high spatial resolution NMR setup will be presented. In chapter 3 the basic chemical aspects of acrylates and curing reactions will be discussed. An introduction into possible network types and the glass transition temperature is given.
Some additional techniques and setups which are used during the research covered in this report are described in chapter 4, together with some additional equipment to heat the sample inside the NMR setup.
In chapter 5 measurements on two acrylate types as well as a triple layered coating sample are shown and discussed. The measurement on the triple layered coating will show the possibilities of the setup to discriminate network properties as a function of position.

Chapter 2

Nuclear magnetic resonance

2.1 Introduction to NMR

The phenomenon of nuclear magnetic resonance (NMR) was discovered in 1946 independently by the two research groups of F. Bloch and E.M. Purcell, respectively[5,6]. NMR is based on absorption of the energy of a radio frequency (RF) pulse by the nuclear spins of the atoms in a material. Every type of nucleus with non-zero spin has a NMR resonance frequency which depends on the strength of the magnetic field surrounding the atom.

2.1.1 Nuclear magnetic resonance

A nucleus with a non-zero spin can have a magnetic moment $\vec{\mu}$. This magnetic moment $\vec{\mu}$ is often associated with the spinning of the charged nucleus. If a magnetic moment is placed inside a magnetic field $\vec{B_0}$, it will tend to align itself along the direction of the magnetic field. A torque $\vec{\tau}$ will be exerted on the magnetic moment.

$$\vec{\tau} = \vec{\mu} \times \vec{B_0}\,, \tag{2.1}$$

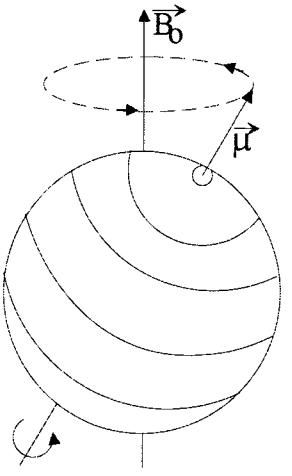

Figure 2.1: *A nucleus with a magnetic moment μ in a magnetic field B_0 precesses at the Larmor frequency.*

which will change the orientation of the magnetic moment

$$\frac{d\vec{\mu}}{dt} = \gamma\vec{\tau} = \gamma\vec{\mu} \times \vec{B}_0 \,, \tag{2.2}$$

with $\gamma/(2\pi)$ the gyromagnetic ratio, which is 42.58 MHz/T for hydrogen. This causes the magnetic moment to precess around the magnetic field (see figure 2.1) with an angular velocity ω_L:

$$\vec{\omega_L} = 2\pi\vec{f_L} = 2\pi\gamma\vec{B_0} \,, \tag{2.3}$$

with f_L the so called Larmor-frequency.

2.1.2 Mathematical description of the nuclear magnetic moment

To describe the motion of the nuclear magnetisation in a mathematical way, it is convenient to work in a frame of reference, which is stationary in terms of the magnetisation vector. To achieve this, a frame of reference (x', y', z) rotating with a frequency ω in the laboratory frame of reference (x, y, z) can be introduced. The z-axis is along the $\vec{B_0}$ magnetic field. For a magnetic moment $\vec{\mu}$ in the laboratory frame of reference, this means for the magnetic moment $\vec{\mu'}$ in the rotation frame of reference:

$$\frac{d\vec{\mu'}}{dt} = \frac{d\vec{\mu}}{dt} - (\vec{\mu} \times \vec{\omega}) \,, \tag{2.4}$$

so that for ω=ω_L, $d\vec{\mu'}/dt = 0$. If a small constant field $\vec{B_1}$ in the rotating frame of reference is applied perpendicular to $\vec{B_0}$, a rotation of the magnetisation about $\vec{B_1}$ is performed. Note that this constant $\vec{B_1}$ field in the rotating frame of reference, represents a field rotating at frequency ω, in the laboratory frame of reference. The rotation of $\vec{\mu'}$ about $\vec{B_1}$ is described by 2.2:

$$\frac{d\vec{\mu'}}{dt} = \gamma\vec{\mu'} \times \vec{B_1'} \,. \tag{2.5}$$

If the field B_1 is known, the so called flip angle θ [rad] of the magnetisation can be calculated:

$$\theta = 2\pi\gamma B_1 t_p, \tag{2.6}$$

where t_p is the duration of the applied field B_1.
The magnetisation of a sample is the sum of all the magnetic moments in the sample:

$$\vec{M} = \Sigma\vec{\mu} \,. \tag{2.7}$$

The macroscopic effects of manipulation and relaxation of the magnetic moments in a sample in the rotating frame of reference are described by the Bloch equations[5]:

$$\frac{dM_{x'}'}{dt} = \frac{-M_{x'}'}{T_2} + \gamma(\vec{M'} \times \vec{B_1'})_{x'} \tag{2.8a}$$

$$\frac{dM'_{y'}}{dt} = \frac{-M'_{y'}}{T_2} + \gamma(\vec{M'} \times \vec{B'_1})_{y'} \tag{2.8b}$$

$$\frac{dM'_{z'}}{dt} = -\frac{M'_{z'} - M_0}{T_1} + \gamma(\vec{M'} \times \vec{B'_1})_{z'} \,. \tag{2.8c}$$

T_1, and T_2 are characteristic time scales for relaxation of the magnetisation along the z-axis, respectively in the xy-plane, to their initial states parallel to the main magnetic field $\vec{B_0}$, after application of a field $\vec{B_1}$. These relaxation processes will be discussed now.

2.1.3 Relaxation processes

Two important relaxation processes for the magnetization after excitation by a B_1 field, are spin-lattice (longitudinal) relaxation along the z-axis, and spin-spin (transverse) relaxation in the xy-plane.

spin-lattice (longitudinal) relaxation At temperatures above absolute zero, all atoms are in motion. The charges associated with the moving atoms create a very complex magnetic field. An atom in this field might experience incidently a frequency equal to its own Larmor frequency. This interaction between the magnetic moment of the nucleus and the fluctuating field, might cause the nucleus to switch its spin state. The energy change of the nucleus, is transferred to the vibrational and rotational energy of atoms and molecules. This effect causes the magnetisation along the B_0 field after excitation, to return to its initial state M_0 with a characteristic time T_1:

$$M'_z(t) = M'_0 \exp(-t/T_1) \,. \tag{2.9}$$

spin-spin (transverse) relaxation The spin-spin relaxation originates from the magnetic field induced by the spins on each other. This will cause each spin to 'feel' a small field superimposed on the B_0 field. Therefore the Larmor frequencies of the individual spins will differ, causing the spin components in the xy-plane ($\perp \vec{B_0}$) to dephase and lowering the transverse magnetisation. This relaxation has a characteristic time T_2. Nuclei in liquids can move more freely, largely averaging out these small magnetic fields. This leads to a longer time scale for T_2 in liquids than in solids.
The effect of the transverse relaxation on the magnetisation M_{xy} in the plane perpendicular to $\vec{B_0}$ is described by:

$$M'_{xy}(t) = M'_{xy}(0) \, \exp\left(\frac{-t}{T_2}\right) \tag{2.10}$$

2.1.4 Frequency Encoding

To obtain spatially resolved information from the NMR signal, a gradient G_y can be superimposed onto the B_0 field. If this gradient is applied in the y-direction,

the magnetic field in the z-direction becomes

$$B_z(y) = B_z(0) + G_y \cdot y \tag{2.11}$$

The Larmor frequency becomes position dependent and equation 2.3 changes into:

$$\omega_L = \gamma B_z(y) = \gamma(B_z(0) + G_y \cdot y)\,. \tag{2.12}$$

Because each frequency in the NMR signal is linked to a position along the y-axis in the sample by the gradient, the Fourier transform of the NMR signal represents the spatial distribution of the NMR signal along the y-direction.

2.1.5 Resolution

The resolution is limited by the resonance line width, which depends on the properties of the Fourier-transform of the original signal in a homogeneous field and the applied field gradient. Besides field-inhomogeneities, essentially three factors limit the maximum achievable resolution for a certain field gradient: the length of the acquisition-window, the transverse relaxation time T_2 and diffusion.
The maximum achievable resolution is linked to the linewidth $\Delta\nu$ in the frequency spectrum by:

$$\Delta z = \frac{\Delta\nu}{\gamma G_z}\,. \tag{2.13}$$

The acquisition window can be viewed as a square pulse of duration t_{acq} in the time domain, which results in a sinc-function with full width at half maximum (FWHM) of $3.8/t_{acq}$ in the frequency domain ν. Hence, the resolution is limited by the length of the acquisition-window to a maximum of

$$\Delta z_{acq} = \frac{3.8}{t_{acq}\gamma\, G_z}\,. \tag{2.14}$$

The second important factor is the sample dependent T_2. Because the received NMR-signal is not purely a signal composed of the signal of the spins rotating at the Larmor frequency but has also an exponentially decaying component, the fourier transformed ($\mathcal{F}$) spectrum will be convoluted with a Lorentzian function:

$$|\mathcal{F}(e^{-t/T_2})| = \frac{1}{\pi}\frac{T_2}{\nu^2 T_2^2 + 1}\,, \tag{2.15}$$

with a FWHM of $1/T_2$ this leads to a maximum resolution of[7]:

$$\Delta z_{T_2} = \frac{2}{\gamma G_z T_2}\,. \tag{2.16}$$

A third factor, especially important in fluids, is limitation of the resolution by self-diffusion. Broadening of the signal line-width due to dephasing of the spins, ans displacement of nuclei to neighbouring pixels plays a role[7,8,37].

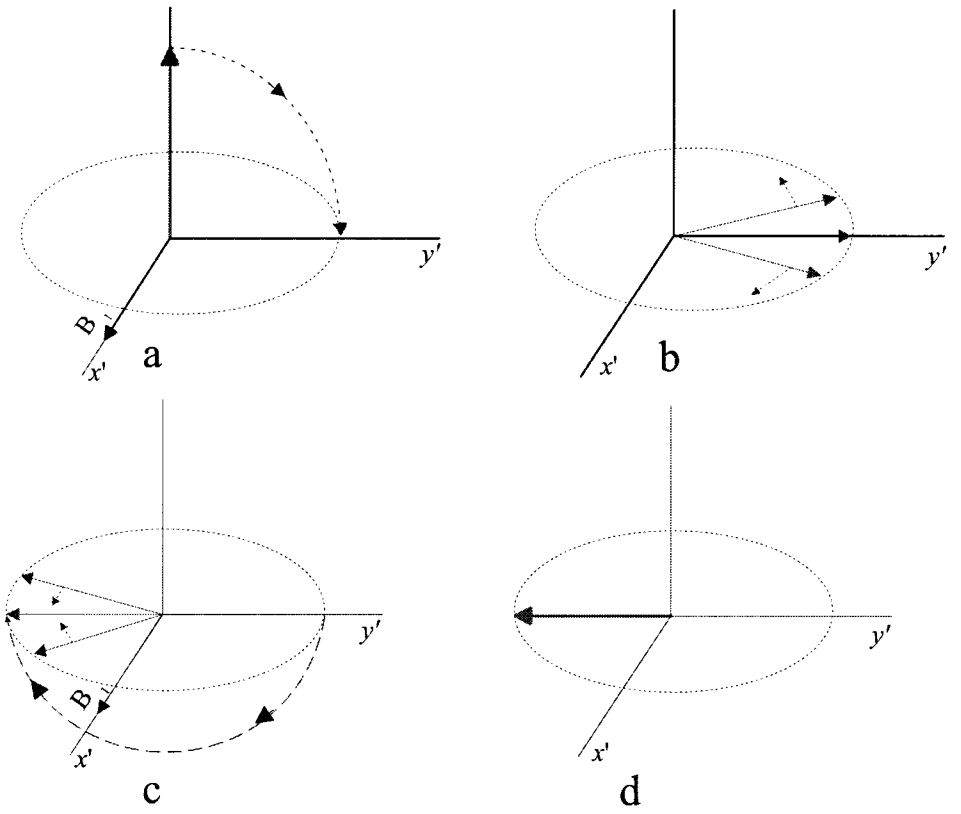

Figure 2.2: *The magnetisation is initially along the z-axis (a), then it is rotated 90° towards the y'-axis, next the spins start to dephase. (b). After a 180° pulse the phase difference is inverted by the pulse (c). The spins start to rephase and finally create an echo (d).*

2.2 NMR pulse sequences

There are several possibilities to manipulate the magnetisation using RF-pulse sequences in such a way, that information on the nuclear density, on T_2, and T_1 can be obtained. The sequences relevant for this report will now be introduced.

2.2.1 Hahn spin echo

The most simple sequence, which forms the base of other more complex sequences is the Hahn-spin echo sequence. In this sequence (shown in figure 2.2) the magnetisation is first rotated into the xy-plane by a 90°-pulse. Next, the individual magnetic moments will start to dephase because of inhomogeneities in the magnetic field or a gradient in an external applied magnetic field. After a time τ, a 180° pulse is applied, after which the magnetisation is inverted. After another time τ, all spins are rephased, giving an echo.

2.2.2 CPMG spin echo train

Instead of just one 180° pulse it is also possible to apply a train of 180° pulses, see figure 2.3. This sequence is known as the Carr-Purcell-Meiboom-Gill (CPMG)

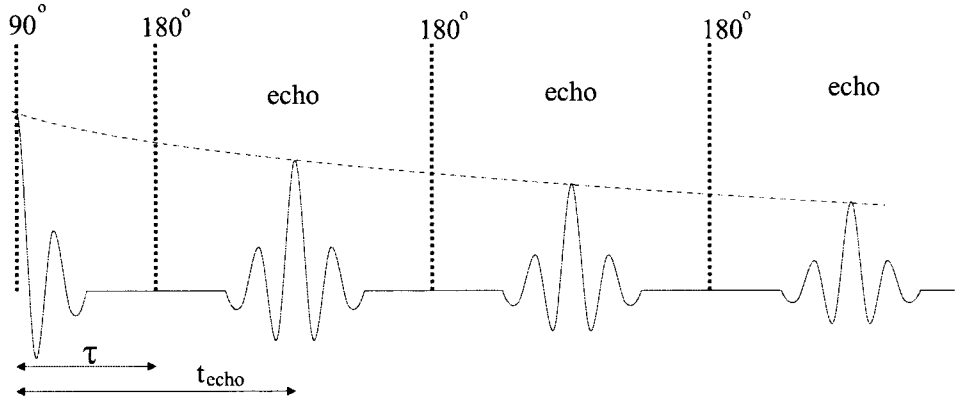

Figure 2.3: *The CPMG sequence consists of a number rephasing 180°-pulses after the initial 90°-pulse. An echo is formed at $t = nt_{echo}$ The echo intensity shows the effect of the transverse relaxation.*

sequence. The time between two echoes, 2τ is called the inter echo time t_{echo}. The echo intensity S_{echo} will decrease because of transverse relaxation

$$S_{echo} = S_0 \exp\left(\frac{-t}{T_2}\right) , \tag{2.17}$$

where $t = nt_{echo}$ is the time since the 90°-pulse, and S_0 is the echo intensity at $t = 0$.

Diffusion measurement The displacement r by (normal) self-diffusion is described by $< r^2 >= 6Dt$, where D is the self-diffusion coefficient and t the time. When a field gradient G is superimposed on the field B_0, it becomes possible to use the CPMG (and Hahn spin echo) sequence for measurements of the (self-)diffusion coefficient of the hydrogen atoms in the sample. The dephasing of spins will not only take place because of local field inhomogeneities, but also because spins move randomly through the sample into areas with a different field strength. The decay of the intensity of the signal now dependents on the diffusion coefficient D. This can be described by adding a diffusion dependent term to equation 2.17, giving for the signal intensity:

$$\ln S \sim \left(-\frac{1}{T_2} - \frac{1}{12}\gamma^2 G^2 D t_{echo}^2\right) t . \tag{2.18}$$

By measuring the signal decay at several different inter echo times t_{echo}, the 'normal' T_2 relaxation can be eliminated and the diffusion constant D can be calculated.

Averaging and long delay It is often common to repeat the CPMG-sequence several times and average the echo signals to increase the signal to noise ratio. Between two CPMG-sequences a long delay (LD) is inserted, during which the magnetisation can relax to its initial state. Generally a long delay of $3T_1$ is sufficient.

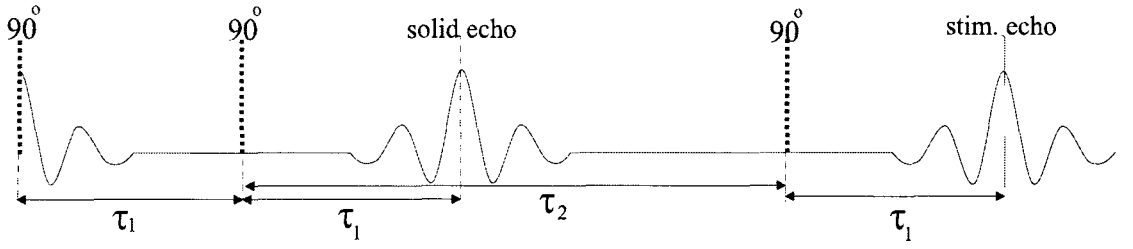

Figure 2.4: *A stimulated echo sequence consists of three 90° pulses and two echoes. The first echo at $2\tau_1$ is in fact the same as the first echo of the OW sequence and is known a the solid echo. A time τ_2 after the second pulse a third 90°-pulse is applied and another echo is formed after another period τ_1.*

2.2.3 Ostroff-Waugh sequence

Especially in high field-gradients, the 90° pulse will excite a wider area of the sample than the 180° pulse. This is caused by the larger excitation frequency bandwidth of the 90° pulse compared to the the 180° pulse, having a longer duration. This limits the suitability of the CPMG sequence in high field gradients, because the area excited by the 90° and 180° pulses is different.
The Ostroff-Waugh sequence[9,10] is closely related to the CPMG spin echo train. The difference is the fact that each 180°-pulse is replaced by a 90°-pulse, where all pulses excite the same area, but the behaviour of the magnetisation becomes more complex. This complex magnetisation behaviour also causes the first echo to have a smaller magnitude, which is 1/2 of the intensity of the first CPMG echo, whereas the intensity of the second and third OW echo is 3/4 of the corresponding CPMG echo[a]. To obtain the proper signal decay, the signal intensity has to be corrected for this variation in echo intensity.
Additionally both the transverse and diffusion-based relaxation, show decay rates different from the ones derived from a CPMG sequence. For a more thorough discussion on the differences, see appendix A.

2.2.4 Stimulated echo sequence

In samples with low diffusion coefficients the use of the CPMG sequence and OW sequence for diffusion measurements is limited because the longest diffusion times which can be obtained are limited by the transverse relaxation time.
A stimulated echo experiment (figure 2.4) results, contrary to CPMG experiments, in an echo decay which is largely governed by the spin-lattice relaxation, which is slower than the spin-spin relaxation.
The spin echo sequence begins with a 90°-pulse which rotates the magnetisation into the xy-plane. In the next part of the sequence the transverse magnetisation is attenuated by transverse relaxation. The second 90°-pulse rotates half of the magnetisation in the z-direction. This second 90°-pulse gives rise to an echo (the

[a] if transverse or diffusion-based relaxation effects are neglected.

solid echo), which is identical to the first OW-echo and has an intensity

$$S_{solid} = \frac{S_0}{2} \exp\left(-\frac{2\tau_1}{T_2}\right) \exp(-\frac{2}{3} D\gamma^2 G^2 \tau_1^3) \,. \tag{2.19}$$

After a time $\tau_2 \gg \tau_1$ a third 90°-pulse is given, which restores the magnetisation stored in the z-direction back into the xy-plane. The magnetisation then evolves into a second echo (stimulated echo) at a time τ_1 after the third RF-pulse.

$$S_{stim} = \frac{S_0}{2} \exp\left(-\frac{2\tau_1}{T_2}\right) \exp(-\frac{\tau_2}{T_1}) \exp\left[-D\gamma^2 G^2 \tau_1^2 (\frac{2}{3}\tau_1 + \tau_2)\right] \,. \tag{2.20}$$

By dividing the intensities of the stimulated echo (eq. 2.20) and the solid echo (eq. 2.19), the T_2-dependence can be eliminated, and this results in

$$\ln\left(\frac{S_{stim}}{S_{solid}}\right) = -\left(D\gamma^2 G^2 \tau_1^2 + \frac{1}{T_1}\right) \tau_2 \,, \tag{2.21}$$

and the diffusion can be calculating by performing experiments at different values of τ_2. If T_1 is not known, the same experiments can be performed with varying τ_1 to eliminate T_1.

2.3 High spatial resolution NMR setup

The NMR setup consists of a field B_0 of 1.4 T with a field gradient G of 36.4 T/m to ensure the spatial resolution necessary for measurements in thin layers of coating. This is achieved using magnet pole tips specially designed for this task, see figure 2.5. The gradient of 36.4 T/m results in a conversion factor of 0.65 μm/kHz from frequency to depth.
The coating sample, which is (usually) applied on a glass substrate, is put slightly ($\sim$ 0.1 mm) above the transmitting and receiving RF-coil, see figure 2.6. The sample holder can be aligned perpendicular to the field gradient $\vec{G}$ using three screws. This has to be done very carefully to get a high depth-resolution in the sample.
The NMR measurement itself can be performed using the NMR-client/server software[11,12] where the required sequence and measurement parameters can be selected.

2.3.1 Heating of the sample in the NMR setup

For NMR measurements on acrylate coatings it is desirable to perform measurements at various temperatures. This way the behaviour of the NMR signal as a function of temperature can be investigated. For some coatings it is necessary to raise the temperature above room temperature to be able to do measurements above glass transition temperature (see section 3.2.)
For this task a setup is build which blows hot air over the sample, see figure 2.7. The airflow can be adjusted and is heated to an adjustable, constant temperature.

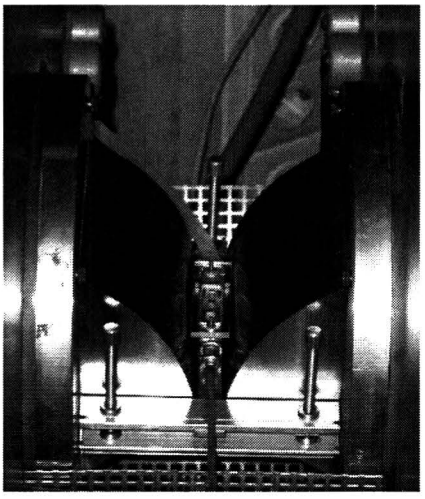

Figure 2.5: *Magnet pole tips and the sample holder of the NMR setup. The pole tips are designed to produce a very high gradient of* 36.4 T/m *to ensure a spatial resolution sufficient for measurements in coatings.*

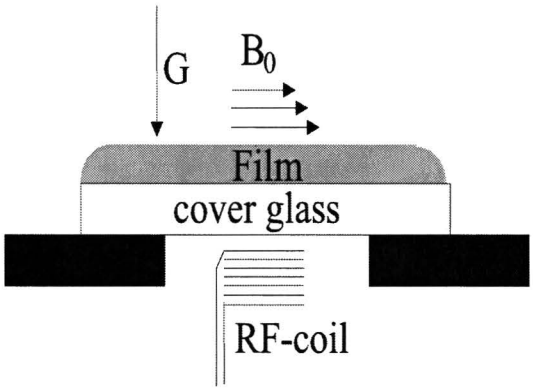

Figure 2.6: *Sample holder of the NMR setup. The coating is applied on a glass substrate (or any other flat, non-magnetic material) and put slightly above the RF-coil. The field gradient G of the field B_0 should be perfectly perpendicular to the substrate.*

The hot air is blown on top of the sample through a pipe with a number of small holes. This creates an homogeneous distribution of hot air possible and minimises vibrations and movements of the sample.
The sample temperature is determined by a thermocouple attached to the sample holder about 2 mm from the sample. Attaching the thermocouple directly onto the sample may cause electrical or vibrational effects which influence the NMR measurement. Attachment at some distance from the sample also ensures that the metal in the thermocouple does not influence the RF-signals or field.

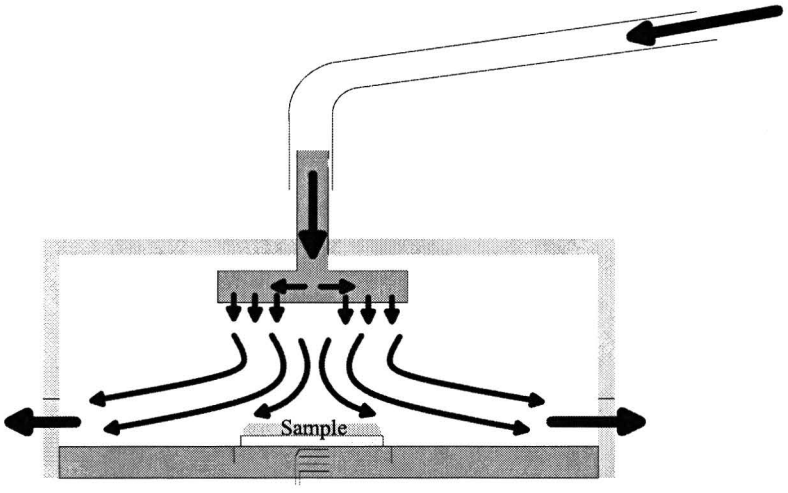

Figure 2.7: *Equipment to heat the sample in the NMR setup consists of a perspex cover that is placed over the sample holder. Hot air is blown on top of the sample through a pipe with a number of holes, which should distribute the air homogeneously. The air is coming from a external heater (not shown) which heats the air to a constant temperature. The temperature can be measured with a thermocouple which has to be secured about 2 millimetres from the sample.*

Chapter 3

UV curable acrylate coatings: Some basics

3.1 Initialization and termination of the curing reaction

Acrylates are organic molecules which contain a $H_2C{=}CH{-}(C{=}O){-}$ group. For UV-curing, the acrylate-monomers have to be mixed with a small (about 1–3 mass-%) amount of photoinitiator. The acrylates 2-ethyl hexylacrylate (EHA), poly(ethyleneglycol) diacrylate (PEGDA), and the photoinitiator 1-hydroxycyclohexyl phenyl ketone (HCPK), which are relevant for this report, are shown in figure 3.1. Several reactions which occur during UV curing are presented now.

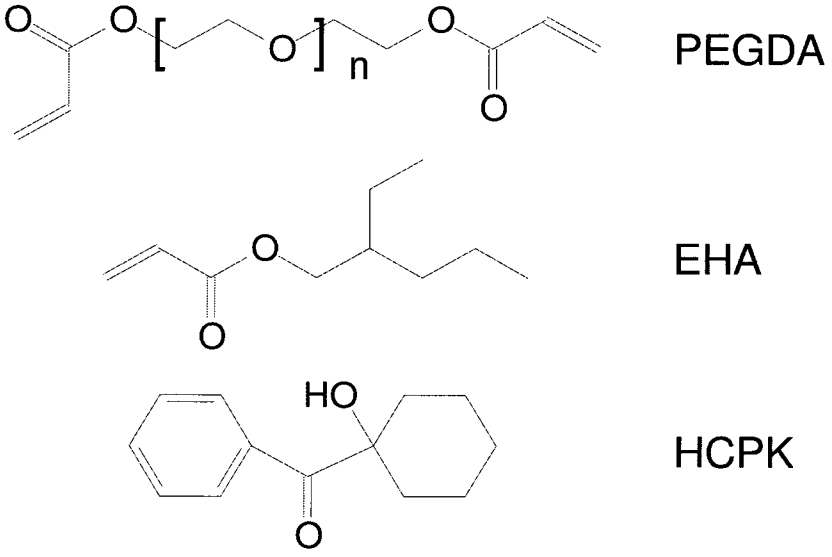

Figure 3.1: *Chemical structures of the compounds relevant for this report: 2-ethyl hexylacrylate (EHA), poly(ethyleneglycol) diacrylate (PEGDA), and 1-hydroxycyclohexyl phenyl ketone (HCKP or Irgacure 184).*

Initiation The photoinitiator splits up into two radicals under the influence of UV-light

$$\mathrm{I{-}J} + \hbar\nu \rightarrow \mathrm{I}\bullet + \mathrm{J}\bullet$$

These radicals react with the double carbon bond of the acrylate M. Because the C=C double bond has opened, but is only replaced with one new bond, the acrylate radicalizes too

$$\mathrm{M} + \mathrm{I}\bullet \rightarrow \bullet\mathrm{M{-}I}$$

Continuation Because the reaction product $\bullet$M−I has a reactivity very similar to the starting radical I$\bullet$[13], the reaction can continue:

$$\mathrm{M} + \bullet\mathrm{M{-}I} \rightarrow \bullet\mathrm{M{-}M{-}I}$$

and further polymerization results in:

$$\mathrm{M} + \bullet\mathrm{M{-}M{-}I} \rightarrow \bullet\mathrm{M{-}M{-}M{-}I}$$

Termination The polymerization process continues until a termination reaction takes place, where the radical reacts with another radicalized acrylate or photoinitiator radical, e.g.:

$$\bullet\mathrm{M{-}I} + \bullet\mathrm{M{-}M{-}I} \rightarrow \mathrm{I{-}M{-}M{-}M{-}I}$$

Hydrogen abstraction abstraction of a hydrogen atom from another molecule by the radical also ends the polymerization, eg.:

$$\bullet\mathrm{M{-}I} + \mathrm{M'H} \rightarrow \mathrm{HM{-}I} + \mathrm{M'}\bullet\,,$$

where M'H = M. If the ratio between hydrogen atoms and acrylate groups increases, the significance of hydrogen abstraction also increases. This is for example the case when increasing the molecular weight in PEGDA, see figure 3.1.

Oxygen inhibition Another possible reaction is oxygen inhibition, where a radical reacts with oxygen. The resulting radical is not reactive towards the acrylate double bonds and can not participate in the polymerization reaction, but usually subtracts a hydrogen atom from other molecules to generate a hydroperoxide[14]. For example:

$$\mathrm{M{-}M{-}I}\bullet + \mathrm{O_2} \rightarrow \bullet\mathrm{O_2{-}M{-}M{-}I}$$

$$\bullet\mathrm{O_2{-}M{-}M{-}I} + \mathrm{M'H} \rightarrow \mathrm{H{-}O_2{-}M{-}M{-}I} + \mathrm{M'}\bullet\,.$$

An additional amount of photo-initiator is needed to consume the oxygen dissolved in a coating before the polymerization process can start. The premature chain-termination and the generation of hydroperoxides modify the mechanical properties of a cured acrylate. The effects of dissolved oxygen can be eliminated by curing in an oxygen-free atmosphere, like N_2.

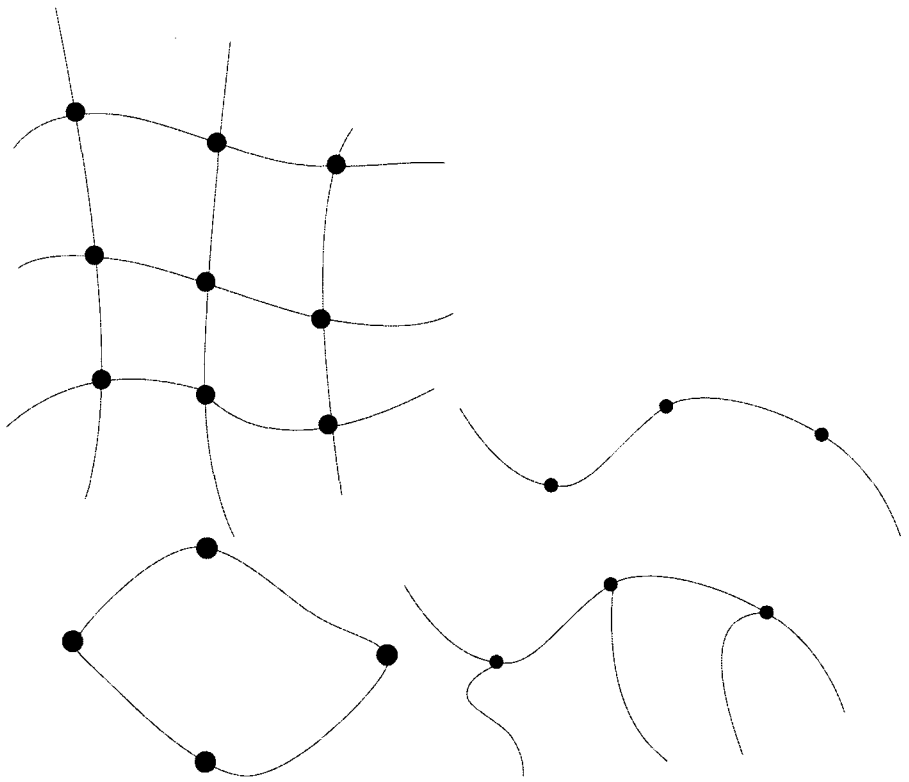

Figure 3.2: *Schematic representation of polymer types: cross-linked network (top-left), linear chains (top-right), closed ring-structures (bottom-left) and branched chains (bottom-right). Combinations of these polymer types like cross-linked networks with linear, dangling ends are also possible.*

3.1.1 Polymer structure formed during the reaction

The properties of the polymer structure formed during UV-curing depend to a large extent on the acrylate-monomers used. Acrylates can have different functionalities (numbers of acrylate groups), e.g. mono- or di-functional. In figure 3.1 EHA is an example of a monofunctional acrylate, while PEGDA is a di-functional acrylate.
This difference in functionality leads to obvious differences in the polymer structure after curing: the monofunctional monomer can only react with two other monomers. This leads to linear chains (figure 3.2, top-right) or, if the chain reacts with its own end, a ring (figure 3.2, bottom-left). In case of side-groups attached to the acrylate (for example in EHA), branched chains (figure 3.2, bottom-right) are formed: A linear main chain (backbone) with branched side chains. Curing of a monofunctional acrylate with side chains can result in a branched structure (figure 3.2, bottom-right.) The di-functional monomer has two functional groups which in total can react to four other monomers, resulting in a rigid, cross-linked network, see figure 3.2, top-left. Monomers with a higher functionality lead to even more complex 3D-networks.
Of course it is possible to cure mixtures of mono- and di-functional acrylates. This can result in linear extensions of the cross-linked network ('dangling chains') and a lower cross-link density than in case of only di-functional acrylate.

3.2 Glass transition temperature

Instead of direct measurements of the network density, the glass transition temperature is often used to characterize the network density of a polymer.
The glass transition occurs in some amorphous materials which do not have the ability to crystallize, as a result of a too irregular structure[15]. Upon heating, these materials transform from a hard glass-state into a more elastic rubbery state at the glass transition temperature (T_g). On a macroscopic level there are a number of changes in properties of the polymer during the glass transition. Upon heating a decrease in stiffness occurs, while there are also changes in heat capacity and thermal expansion coefficient.
These changes in properties at the glass transition temperature can be measured by differential scanning calorimetry (DSC) or thermo mechanical analysis (TMA). These techniques respectively record the heat capacity and the volume as a function of temperature. For more details, see section 4.2.
On a microscopic scale, the glass transition temperature can be viewed as the temperature where the internal mobility reaches the value which is characteristic for the time scale of the experiment[16]. In other words: the polymer structure can be viewed rigid below and mobile above the glass transition temperature. Therefore it can be intuitively argumented that a more rigid polymer structure will need a higher thermal energy and hence a higher temperature to get a mobility high enough to reach the time scale of the experiment. It also implies that the measured glass transition temperature depends up to some degree on the duration of the measurement. Glass transition temperatures which have to be compared have to be measured in the same way.
It can be shown[3,16,17,18] that for polymers with sufficiently high molecular weights the glass transition temperature is a function of the chain length between two cross-links, M_c[a]

$$T_g(M_c) = T_g(\infty) - \frac{K}{M_c}\,, \tag{3.1}$$

where $T_g(\infty)$ is the glass transition temperature in case of infinitely long chains and K is a constant. This relation makes it possible to get insight into the cross-link density of a polymer network by measuring the glass transition temperature.

3.3 NMR signal of polymers

In homogeneous coatings information related to the cross-link density can be obtained from measurements of the glass transition temperature. The goal of this report is to obtain similar depth resolved information on the cross-link density from NMR measurements. Because of the strong dependence of the spin-spin relaxation on the mobility of the hydrogen atoms, the transverse relaxation time T_2 can yield valuable information on the polymer structure of a coating.
Gotlib et al.[19] investigated the behaviour of T_2 of cross-linked polymers. Above

[a] Although it is common to refer to this value as chain length, it actually is the molecular weight between two cross-links.

the glass transition temperature they found an increase of T_2 as a function of temperature. When raising the temperature even further they reported a plateau of constant T_2. This constant T_2-value depends on the cross-link density. They explained this behaviour with a model in which the cross-links are fixed. The motion of the chain between two cross-links is anisotropic because of restrictions imposed by these cross-links. Upon heating the motion increases, averaging out dipole-dipole interactions, resulting in a longer T_2. At some temperature all dipole-dipole interactions which can be averaged out by the motion are averaged out. At this point T_2 is governed by dipole-dipole interactions which can not be averaged out because of the anisotropic nature of the motion. A further increase in temperature will not result in a further increase in T_2. Because the anisotropy of the motion depends on the distance between the cross-links, this constant T_2-value is a function of cross-link density ρ_c[19,20]:

$$T_2 \propto \frac{1}{\rho_c} . \tag{3.2}$$

The relation between T_2 and the cross-link density has been further investigated by Litvinov and Dias[4] on EHA/PEGDA mixtures in a NMR relaxometer. They show a clear relation between the glass transition temperature and the NMR T_2-relaxation. A bi-exponential signal decay was reported in this study. They, as well as Simon et al.[21], suggest that the short relaxation time is related to hydrogen atoms between cross-links. The longer relaxation time is associated with highly mobile components like dangling chains and network defects such as free linear chains or loops.

It is possible to obtain information on the hydrogen density in a coating from the magnitude of the NMR signal. This enables one to measure changes in the proton-density, for example to measure the moisture content during a drying process of a water or solvent borne coating. The UV curing process is very fast and there is no change in hydrogen density during the UV curing of acrylates. This means that for the UV cured acrylates used in this report, the possible information derived from hydrogen density measurements is limited compared to T_2-analysis.

Chapter 4

Additional techniques

Whereas this report mainly focusses on NMR, there are other techniques which can be used to help interpreting the NMR-data. Confocal Raman-Microscopy (CRM) is used to obtain information on the chemical composition before and after curing of a sample and to measure the degree of double bond conversion. Thermal techniques like Differential Scanning Calorimetry (DSC) and Thermo Mechanical Analysis (TMA) are used to measure the glass transition temperature of a sample.

4.1 Raman spectroscopy

Confocal Raman-Microscopy can be used to identify molecules and specific groups in a sample. Confocal Raman microscopy is chosen instead of the more conventional and well-known technique of infrared (IR) spectroscopy because it can provide depth resolution. CRM is also less sensitive to signal absorption by glass, which is important for coatings on glass substrates. The obtained spectra are very similar to spectra obtained with infrared spectroscopy.
Raman spectra are obtained in a non-destructive way, by measuring the spectrum scattered by a sample exposed to a light source. For Raman spectroscopy, a monochromatic light source is used and in the sample the following physical phenomena can occur:

- If an incoming photon has enough energy, it can excite an electron and the applied radiation is absorbed. The excitation energy of the electron is radiated back, the so-called **fluorescence**, or converted into heat.

- In case of **Rayleigh scattering**, a part in the order of 10^{-4} of the incident radiation is scattered back by elastic collisions of the photons with the molecules of the sample. In this case the scattered energy and hence the frequency remains the same.

- In case of **Raman scattering**, a fraction (about 10^{-8}) of the incident light is scattered back inelastically. Because of the inelastic nature of the collision, the backscattered light has a frequency different from the incident light,

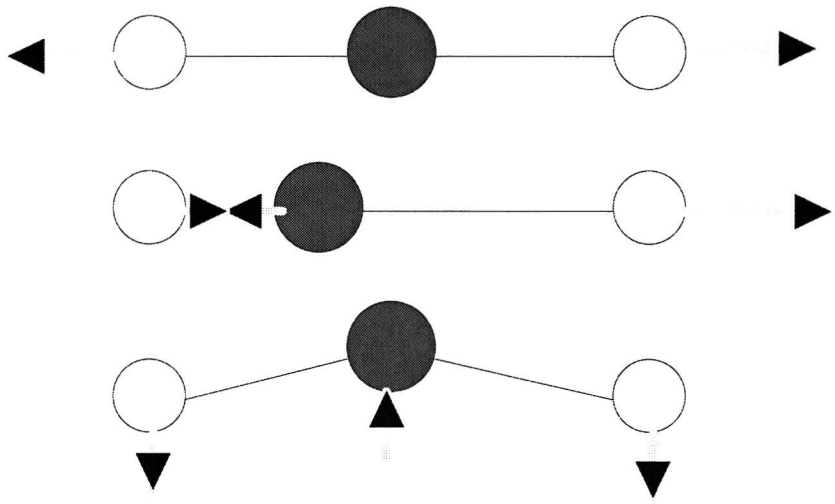

Figure 4.1: *Several vibration modes: symmetric and asymmetric stretching and a bending mode. All can be Raman-active.*

where the frequency difference corresponds to the vibrational frequencies of the molecule.

The latter phenomenon is used in Raman-spectroscopy, in which the energy-levels of molecules are explored by examining the frequencies present in the scattered radiation. The energy difference between the incident and scattered radiation is used to increase the vibrational or rotational energy of the molecules. However, the opposite is also possible: upon collision with the incident photon, the molecule goes to a lower rational or vibrational level and the scattered photon has a higher energy than the incident photon. This causes anti-Stokes lines.
Because in both cases the energy differences are quite small, monochromatic light has to be used for the incident radiation to prevent obscuring of the backscattered spectrum by the incident light. Because only a very small fraction of light is scattered, the incident source has to be intense.

4.1.1 Rotational and vibrational Raman spectra

The selection rule for rotational Raman transitions is that the molecule has to be anisotropically polarizable[22]. This means that the polarisation has a directional preference. This includes all linear and diatomic molecules, but excludes spherical rotors like CH_4.
The selection rule for vibrational Raman transitions is that the polarisability of the molecule has to change as the molecule vibrates. See for example figure 4.1. This includes all types of diatomic molecules. During a period of the vibration, the attraction between the nucleus and the electron varies, which changes the polarisability of the molecule.
Once the Raman of a substance is recorded, spectra in literature (e.g. Nyquist[23]) can be used to relate certain peaks to the chemical composition of the substance.

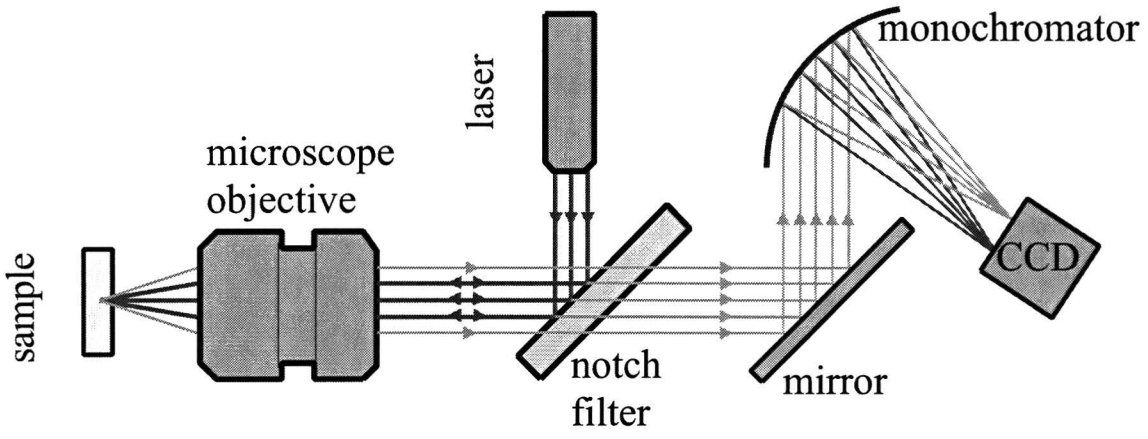

Figure 4.2: *Schematic representation of the confocal Raman microscopy setup. The laser beam (632 nm) is diffracted by a notch filter and then focussed inside the sample by an objective. The Raman-scattered light is lead through the notch filter and a mirror to a monochromator. The monochromator separates all wavelengths in the Raman scattered light, and the resulting spectrum is recorded.*

4.1.2 Confocal Raman microscopy setup

The Raman microscopy setup is schematically represented in figure 4.2. The laser beam is focussed inside the sample. By changing the point of focus to different positions inside the film it is possible to obtain Raman-scattered light from various positions inside the film. The wavelengths in the Raman-scattered light are separated by a monochromator and recorded. The spectral information is processed by a computer system.

4.2 Thermal techniques

Thermal analysis techniques are useful for the study of the polymer structure. Differential Scanning Calorimetry (DSC) and Thermo Mechanical Analysis (TMA) are used in the measurements covered in this report. Both techniques have in common that the sample gets heated (or cooled) during the measurement, while some property of the sample is measured.
DSC records the heat capacity as a function of temperature and is used to obtain information on the glass transition temperature and phase or chemical transitions. TMA probes the mechanical properties like elasticity and sample size as a function of temperature, which also can be used to determine the glass transition temperature.

4.2.1 DSC

A DSC setup contains two crucibles on top of a furnace, of which one crucible contains the sample, while the other crucible is empty and acts as a reference, see figure 4.2. In a DSC measurement, the heat flow to the sample (which is the heat flow to the container with the sample minus the heat flow to the reference

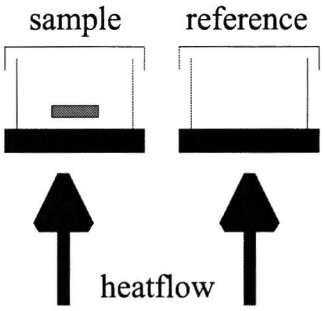

Figure 4.3: *A differential scanning calorimeter (DSC) contains two containers, of which one contains the sample. The second container is used as a reference. The DSC measures the heat flow to each container. The two flows are subtracted, and the difference results from the sample.*

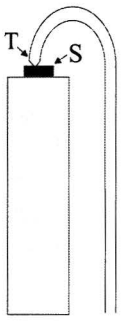

Figure 4.4: *A TMA is based on a tip (T) touching the sample (S) with a certain pressure or force. The thickness of the sample is recorded as a function of the temperature. This type of measurement can reveal properties like thermal expansion coefficient and elasticity.*

container) as a function of the temperature is recorded.
A DSC uses the Boersma principle[24] to measure the heat flow. In this type of system, the temperature drop over an element with a known heat resistance is measured to calculate the heat flow. In this very simple system the heat flow is given by:

$$\phi = \frac{\Delta T}{R} \tag{4.1}$$

During a measurement the furnace heats up, and the heat is transported through the ring with thermophile to the sample and reference container. The power of the furnace is automatically adjusted to keep a certain rate of heating. To measure below room temperature, an intracooler is connected to the DSC. This intracooler always cools the system, while the DSC furnace heats the sample against the cooling.
The recorded data can be processed using computer software to find phase transitions or to calculate the enthalpy change of a reaction.

4.2.2 TMA

In thermo mechanical analysis (TMA), the mechanical properties of a sample are investigated. A TMA system is based on a tip exerting a certain force on the sample. The thickness of the sample under influence of this force is recorded as a function of temperature, while the sample is heated, see figure 4.2.

4.2.3 DSC and TMA setup

The thermal analysis of the coatings is performed with a setup consisting of a Mettler-Toledo DSC822^e differential scanning calorimeter and a Mettler-Toledo TMA40 thermo mechanical analyzer. Both are connected to a computer with the Star software package necessary for the recording and analysis of the data.
The DSC is connected to an intracooler to be able to perform measurements below room temperature, with a minimum temperature of $-65\,°C$. Measurements below

room temperature with the TMA can be performed using a 'cooling finger', a container surrounding the sample that can be filled with liquid nitrogen.
In both cases the rate of cooling can not be adjusted and the temperature is controlled purely by the amount of heating counteracting the cooling. Using the measuring software it is possible to set the start and end temperature as well as the rate of heating. In case of the TMA also the force on the sample can be adjusted.

Chapter 5

Experimental results

In this chapter some experimental results will be presented and discussed.
In section 5.1 the inevitable heating of a sample by RF pulses will be described. The results presented in this section will partly determine the NMR settings in the following sections.
In section 5.2 the properties of the polymer structure of UV cured PEGDA will be reported. These properties were investigated by measuring the glass transition temperature and T_2 relaxation times.
In section 5.3 measurements are presented that were performed on a triple layer poly-urethane sample, to investigate if polymer structure properties like the glass transition temperature can be obtained as a function of depth.
In section 5.4 measurements on UV cured EHA, which does not form a cross-linked network, are presented.

5.1 Heating of the sample by RF-pulses

As was already discussed in section 3.3 the network properties of polymers can be investigated by measuring the transverse relaxation time T_2. A factor influencing T_2 is the temperature. Upon heating the mobility in a polymer increases, increasing the motional averaging of dipolar interactions, resulting in an increasing T_2. So during an experiment it is important to maintain a constant temperature.
An unwanted but inevitable source of temperature increase is formed by the RF-pulses during a measurement. A temperature increase caused by RF pulses can be observed by a dependence of T_2 on the duration of the long delay (LD), see figure 5.1. When LD is decreased, a higher duty cycle of the RF amplifier will result in more energy transmitted by the RF coil. During the pulse-sequence the sample heats up and during the long delay the sample cools down again. The (average) number of pulses per second is to a good approximation given by:

$$\frac{n_{echoes}}{n_{echoes}t_{echo} + LD}, \tag{5.1}$$

where n_{echoes} is the number of echoes in the sequence, t_{echo} the inter echo time and LD is the duration of the long delay.

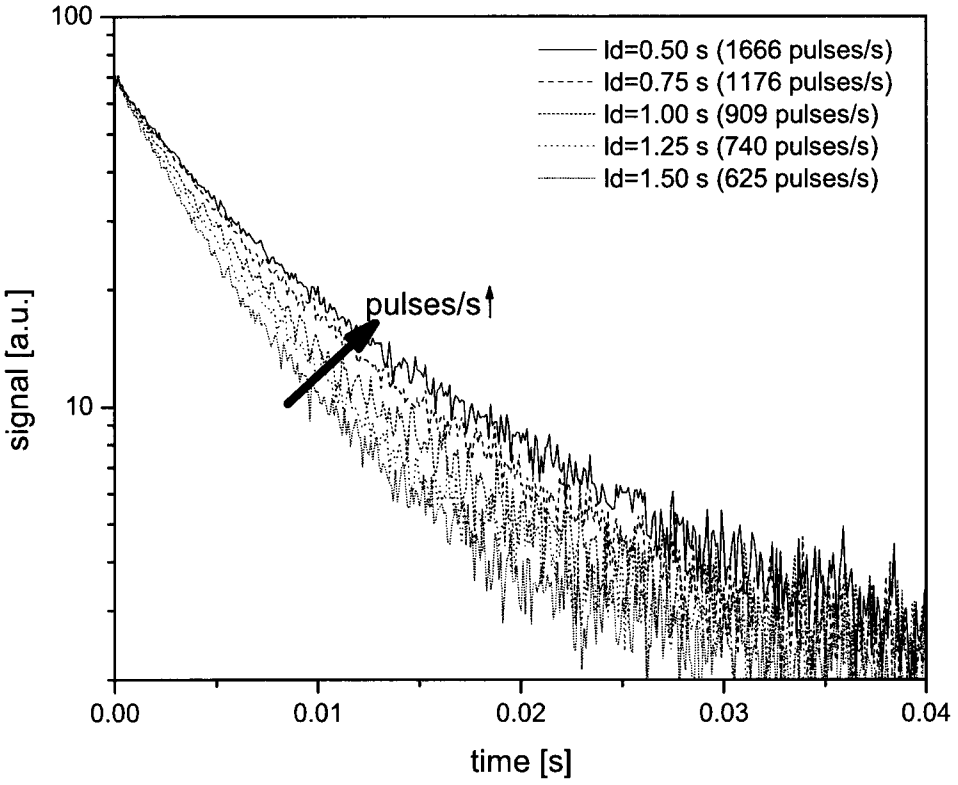

Figure 5.1: *NMR signal decay of UV cured EHA measured as an OW sequence. Decreasing the LD increases the number of pulses per second and the temperature of the sample, which results in a slower decay of the signal.*

n_{echoes}	LD (s)	pulses s^{-1}	effective duty cycle (%)
500	0.45	1000	0.1
1000	0.90	1000	0.1
2000	1.80	1000	0.1
1000	0.40	2000	0.2
2000	0.80	2000	0.2
250	0.475	500	0.05
500	0.95	500	0.05
1000	1.90	500	0.05

Table 5.1: *Settings for the long delay and the number of echoes (n_{echoes}) of an OW sequence used to study the effect of LD on the temperature. An inter echo time of 100 μs is used. The settings are varied in such a way, that they result in three different values for the average number of pulses per second. The resulting decay curves of the measurements with these settings are shown in figure 5.2.*

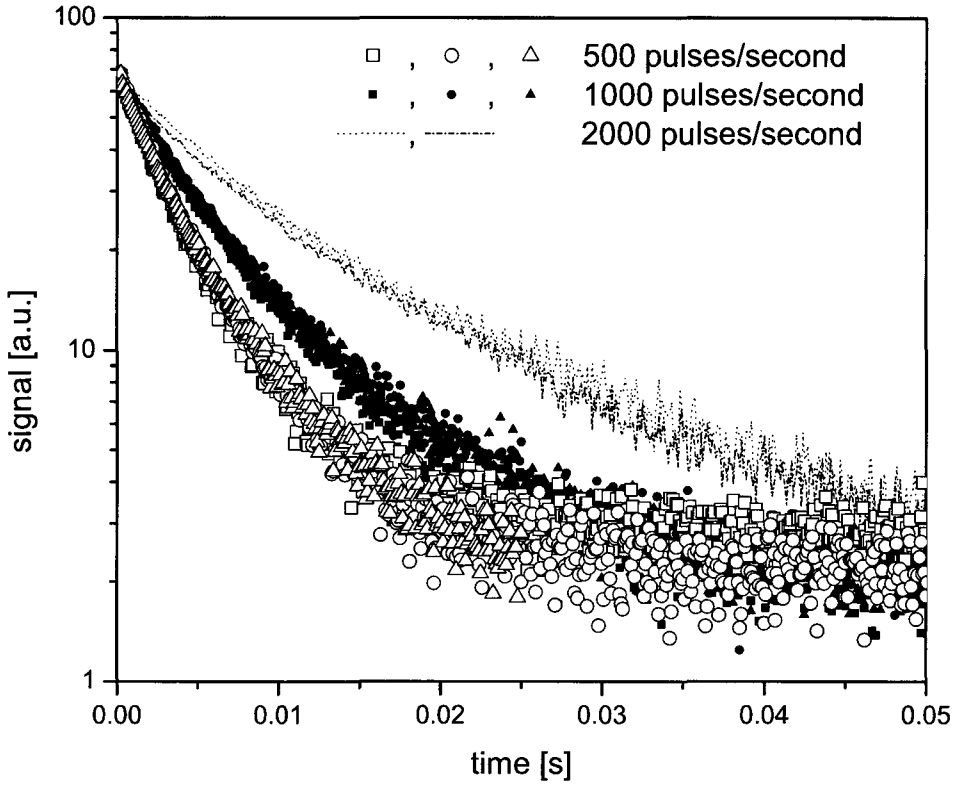

Figure 5.2: *Decay curves for UV-cured EHA. The number of echoes per second and the long delay have been varied according to table 5.1. Groups of decay curves are visible: each for settings with a certain number of pulses per second.*

To investigate the effect of LD on the temperature, a number of measurements with varying combinations of long delay and number of echoes (see table 5.1) are performed . The combinations in table 5.1 are chosen in such a way that several combinations result in an equal number of pulses per second. This is necessary to exclude the possibility that the LD dependence of T_2 is not a temperature effect. The resulting decay curves are shown in figure 5.2. This figure reveals that the combinations from table 5.1 with the same duty cycle lead to similar decay curves, resulting in three groups of decay curves. This indicates that the LD dependence of the relaxation rate for various pulse settings is indeed caused by a temperature increase. Although the heating-process itself has not been investigated, it is likely that thermal radiation from the heated RF-coil plays the most important role because the coil is close ($\sim 100\,\mu$m) to the sample.
To quantify this increase in temperature during the measurement, a glass substrate with a layer of cured PEGDA 575 (ca. 200 μm thick) is used. A fluor optic temperature sensor (Luxtron FOT labkit) with a surface contact probe is placed on top of the sample, centered above the RF-coil.

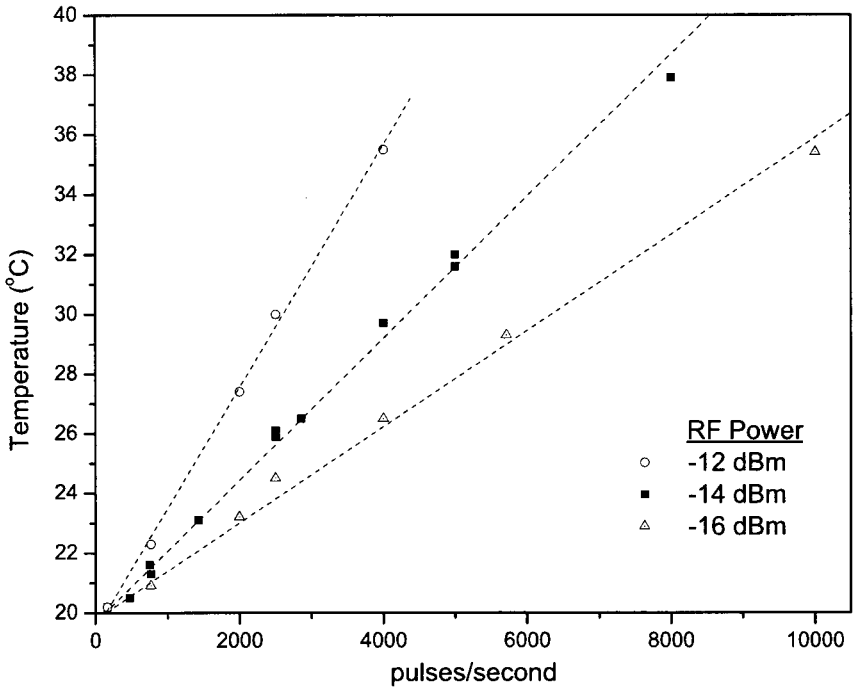

Figure 5.3: *The heating of the sample plotted against the effective duty cycle of the RF coil. The RF Gain setting has been varied.*

The temperature is measured as a function of the number of RF pulses per second. This measurement is performed with 1 μs pulses. The temperature is found to increase linearly with the number of pulses per second, see figure 5.3. The temperature increase is measured for three values of the RF signal power, varying the intensity of the pulses. The temperature increase has been linear fitted and is shown in table 5.2 as a function of the number of pulses per second.

5.1.1 Experimental consequences

The results in figure 5.2 show that the effect of heating of the sample by RF pulses can be compensated by keeping the number of pulses per second constant. When comparing measurements on the same sample this is important, because variation of the inter echo time also leads to a variation in number of pulses per second and the degree of heating. The heating of the sample may lead to a variation in T_2. This variation in T_2 might be interpreted incorrectly.
When comparing measurements on several samples of varying thickness and materials, additional factors influencing the temperature increase have to be taken into account, e.g. the heat capacity, heat conduction, and the size of the sample. These factors are much harder to compensate for than the number of transmitted RF pulses per second. Therefore it is recommended to use a small number of

RF power [dBm]	Temp. increase [10^{-3}K/(pulses s^{-1})]
-12	4.1
-14	2.4
-16	1.6

Table 5.2: *The temperature increase as a function of the RF output. 1μs pulses are used pulses.*

pulses per second. This way the heating as well as the variation in temperature increase between samples are kept to a minimum.
In the measurements presented in the following sections the considerations mentioned above have been taken into account: the average number of pulses is kept constant at 1176 s^{-1}, resulting in an average duty cycle of 0.12%.

5.2 PEGDA

A way to investigate and understand the basics of the relation between the NMR signal and cross-link density of a compound is to vary the cross-link density using similar chemicals. Thereby the number of variables in the experiment is limited as much a possible. A possible compound for this experiment is PEGDA, an acrylate with oligomers of different chain length between the acrylate groups, see figure 3.1. With this substance the distance between cross-links can be varied while the type of the chemical composition remains the same. PEGDA oligomers with molecular weights of 258, 302, 575 and 700 g/mol are commercially available from Sigma-Aldrich Co.

5.2.1 Sample preparation

The uncured PEGDA oligomers are mixed with 1 mass$-$% HCPK (Irgacure-184) photo initiator. After application onto a glass substrates, but before curing, the samples are exposed to a nitrogen atmosphere for 15–20 minutes to minimise the amount of oxygen dissolved in the samples. This is necessary to prevent oxygen inhibition (section 3.1). After 30 seconds of exposure to UV radiation in the nitrogen atmosphere, samples with an average thickness between 100 μm and 300 μm were created.

5.2.2 Degree of curing

PEGDA-700 Raman-spectra of PEGDA-700 before and after curing have been recorded and are plotted in picture 5.4. The Raman-spectrum after curing is recorded approximately five minutes after curing. The most important peaks have been identified using known spectra from the literature[23]. Because no spectra of PEGDA-700 are available in the literature, the spectra of similar chemicals with the same types of groups were used.

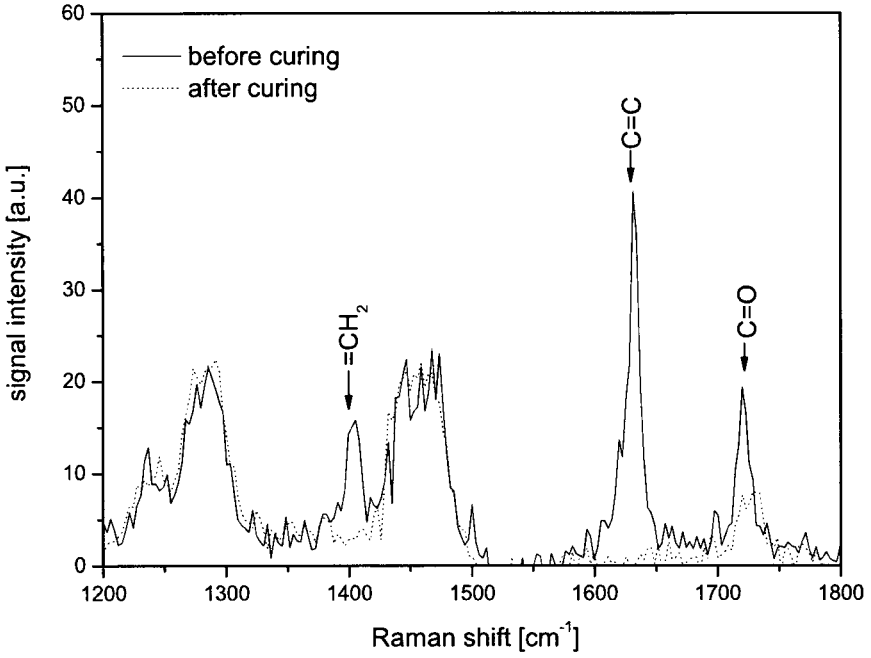

Figure 5.4: *The Raman-spectra of PEGDA 700 before and shortly (ca. 5 minutes) after curing. The peak associated with the –C=C– bonds completely disappears.*

The most obvious difference between the two spectra is the complete disappearance of the peak related to the –C=C– bond. This confirms that during curing cross-links are formed by opening of this bond. There is no remaining signal of the –C=C– bond after curing and the conversion can be assumed to be complete. Another difference between the two spectra is the decrease in intensity of the -C=O peak after curing. The decrease in intensity can be caused by the changed molecular structure after curing, or, although no indication for a reaction with the –C=O bonds could be found in literature, by a reaction of –C=O bonds.

PEGDA-258 PEGDA-258 is the PEGDA oligomer with the lowest molecular weight, resulting in the most dense network structure of the used PEGDA oligomers. Because the curing takes place below the glass transition temperature of the final network (see section 5.2.3), the mobility during curing decreases dramatically, and as a result part of the –C=C– double bonds may not react. Therefore the degree of double bond conversion for PEGDA-258 was measured, see figure 5.5.
Contrary to PEGDA-700, still a signal from the –C=C– bond remains after curing. This remaining signal accounts to approximately 8% of the initial number of –C=C– bonds, which corresponds to a conversion factor of 92%. This percentage is also in fair agreement with Priola et al.[3], they reported a conversion factor of 94% for PEGDA-258 and full conversion for all higher molecular weight oligomers.

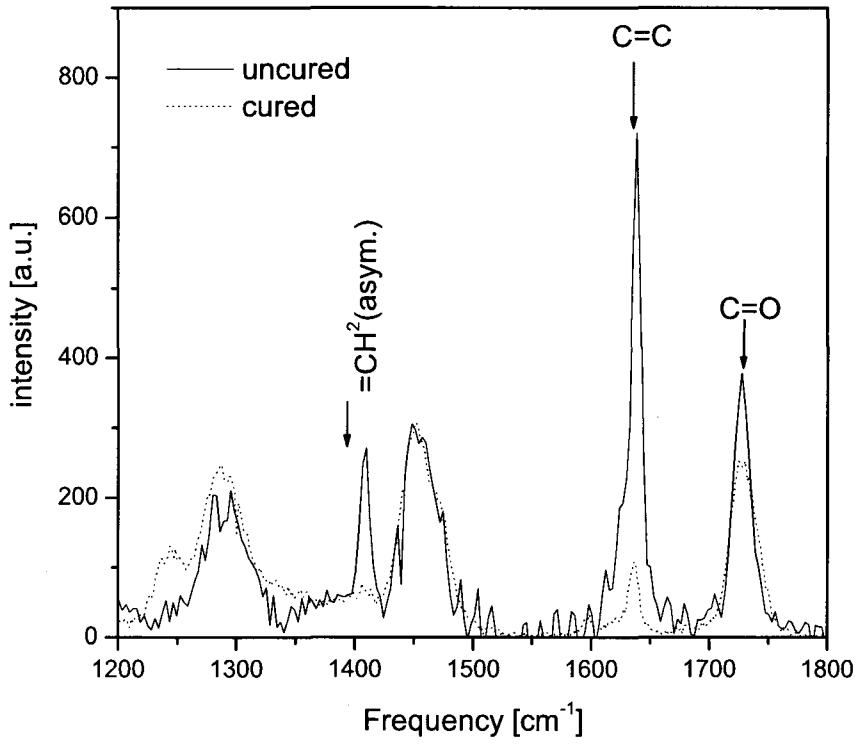

Figure 5.5: *Raman spectrum of the region with the -C=C- and -C=O bond signals of PEGDA-258 before and after curing. Contrary to PEGDA-700 still approximately 8% of the initial -C=C- double bonds are left after curing. The spectrum has been recorded about 24 hours after curing.*

5.2.3 Glass transition temperature

The glass transition temperature T_g of the UV cured PEGDA samples has been measured with a DSC and a TMA, the results are summarised in table 5.3. The chain length is given by:

$$M_c = M_w - 54\,\frac{\mathrm{g}}{\mathrm{mol}}\,, \tag{5.2}$$

where M_w is the molecular weight and 54 g/mol is the weight of the two C_2H_3 groups on both ends of the PEGDA molecule, which do not constitute part of the chain between the cross-links. The reciprocal chain length is plotted against the glass transition temperature in figure 5.6. The relation between M_c and T_g for PEGDA shown in this figure is in agreement with equation 3.1, which predicts a linear dependence. Assuming equation 3.1 is valid, the correspondence of the measured glass transition temperatures of the samples with this equation gives an indication for the quality of the samples.

The extrapolation of the data in figure 5.6 to $M_c^{-1} = 0$ corresponds to the glass transition temperature of PEGDA networks with infinitely long chains. The value found from this extrapolation (−100 °C) is lower than the value given by Priola

M_w	T_g[°C] TMA	T_g[°C] DSC
700	−55	(*)
575	−34	−26
302	33	34
258	(*)	64

Table 5.3: *Glass transition temperatures of UV cured PEGDA oligomers with different molecular weights M_w. Measurements with TMA and with DSC are tabulated. (*) indicates that the values could not be measured with the setup used.*

et al.[3] (−66 °C). However, it is in agreement with the temperature range known for poly(oxy ethylene)[25]. Poly(oxy ethylene) ($[C_2H_4-O-]_n$) is identical to the chain between the acrylate groups in PEGDA, see figure 3.1. Therefore, infinitely long PEGDA chains with negligible fraction of cross-link groups can be viewed as poly(oxy ethylene).

5.2.4 T_2 around the glass transition temperature

Polymer chains in the glass state are considered to be immobile compared to the rubber state, so one would expect large differences in transverse relaxation between both phases. Indeed, a much faster NMR signal decay is observed when going from a rubbery state to a glassy state, as shown in figure 5.7. The data sets plotted in this figure are recorded at room temperature, where PEGDA-575 and 700 are in a rubbery state, while PEGDA-258 is in the glass phase. PEGDA-575 and 700 both have a decay with a relaxation time in the order of ms, the decay of the NMR signal of PEGDA-258 is much faster (< 0.1 ms.)

The difference in NMR relaxation behaviour above and below glass transition temperature makes it interesting to measure T_2 at temperatures around the glass transition temperature. Such a measurement can provide insight into the increase in mobility of the components of the polymer during heating near the glass transition temperature. It also can provide insight into the presence and temperature range of a plateau of constant T_2 (section 3.3).

The PEGDA oligomer of choice for NMR measurements below and above the glass transition temperature is PEGDA-302. The T_g of 34 °C of PEGDA-302 is within the range of temperatures to which the NMR setup can be heated. The T_2 distribution of this polymer as a function of temperature is shown in figure 5.8. Below and just above the glass transition temperature the relaxation is mono-exponential with a T_2 in the order of 0.1 ms. At 20−30 °C above the glass transition temperature a second T_2 component appears. The relaxation now consists of a longer T_2 component (T_2^{long}) and a short (T_2^{short}) component. Litvinov and Dias[4] and Simon et al.[21] distinguish also two T_2 components. They assume that the short component originates from the chains between cross-links, whereas they assume that the long component originates from dangling and linear chains and loops.

T_2^{short} is shown as a function of temperature in figure 5.9. At temperatures be-

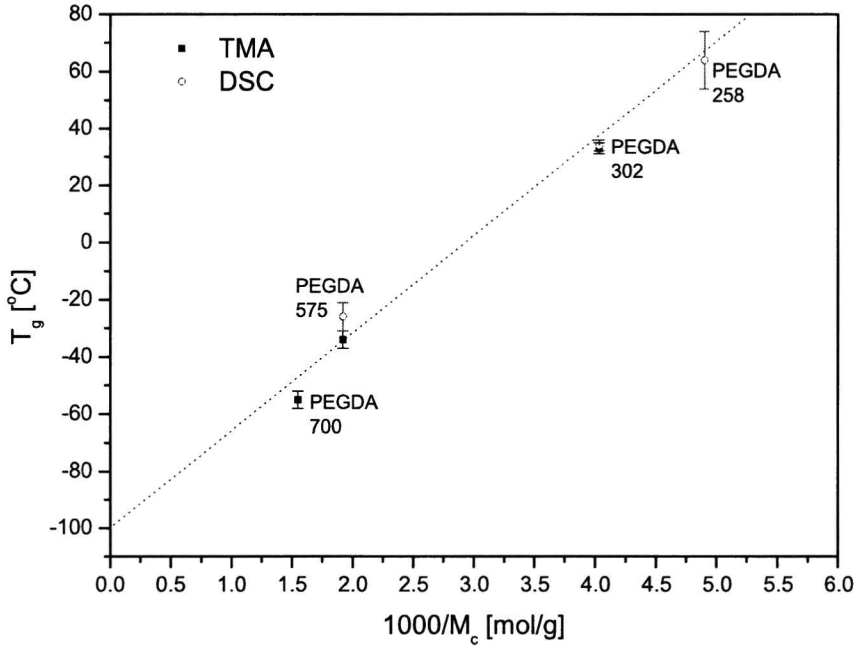

Figure 5.6: *Glass transition temperature as a function of the reciprocal chain length M_c^{-1}. The measurements of T_g by means of DSC as well as by TMA are shown. The error bars are estimates.*

tween the glass transition temperature and approximately 65°C, T_2^{short} is smaller than the inter echo time (50 μs) and can not therefore not be determined correctly. At temperatures between approximately 65 °C and approximately 90°C, $\ln(T_2^{short})$ is inversely proportional to T, where T is the temperature in Kelvin. This dependence can be rewritten as:

$$T_2^{short} \propto \exp\left(\frac{-E_0}{k_B T}\right) \tag{5.3}$$

with a E_0 a constant energy and k_B Boltzmann's constant, indicating a thermal activation with some energy barrier E_0 of the motions responsible for averaging of the dipole-dipole interactions. E_0 can be determined by:

$$\frac{d\ln(T_2)}{d(T^{-1})} = \frac{-E_0}{k_B}\,, \tag{5.4}$$

resulting in $E_0/k_B \sim 10^3$ K.
The plateau of constant T_2^{short} starts at (92 ± 8)°C. The value of T_2^{short} on this plateau is a function of the cross-link density.

5.2.5 Dependence of T_2 on T_g

A relation between the glass transition temperature and the NMR signal decay time T_2 has already been reported by Litvinov and Dias[4] for UV cured

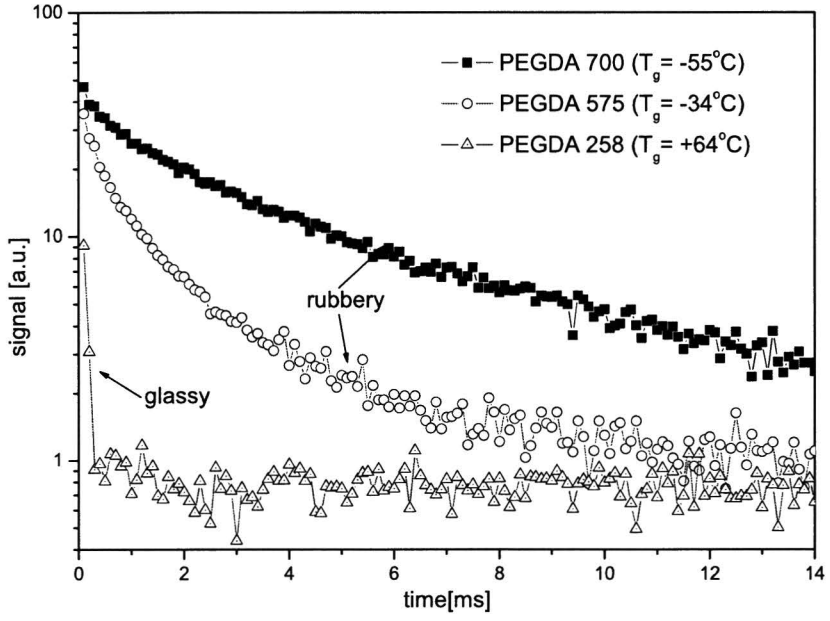

Figure 5.7: *NMR signal decay of PEGDA-258, 575, and 700 measured at room temperature.*

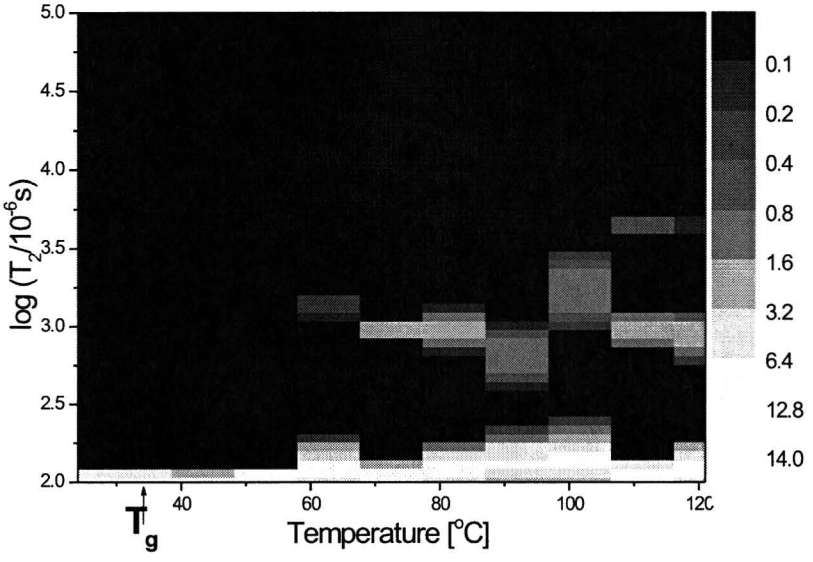

Figure 5.8: *T_2 distribution of PEGDA-302 around its glass transition temperature. Below the glass transition the relaxation behaviour is very fast, whereas at temperatures about 20 °C above the glass transition a slower T_2 component appears. The grey-scale indicates the intensity of the T_2 component.*

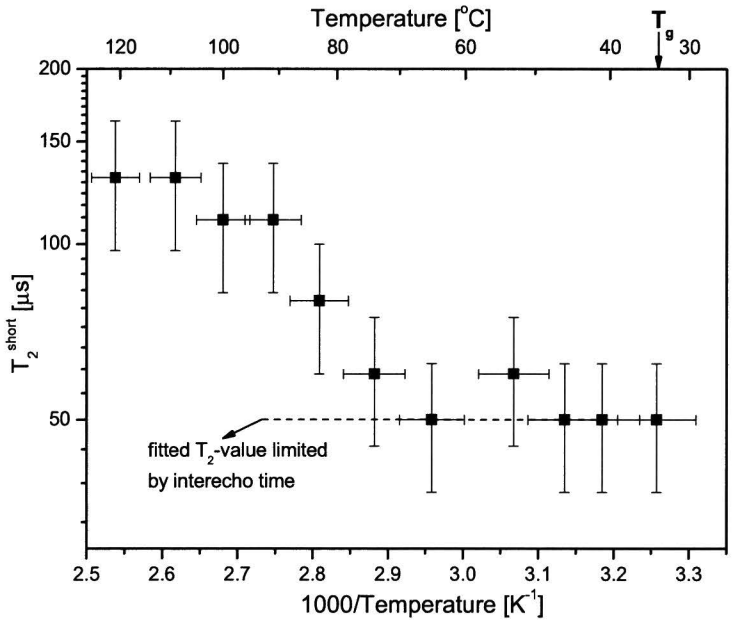

Figure 5.9: *Short component T_2^{short} of the spin-spin relaxation of PEGDA-302 as a function of the reciprocal temperature. T_2^{short} is on a logarithmic scale. At high temperatures, a plateau of constant T_2 is reached.*

EHA/PEGDA mixtures. To test this for the PEGDA oligomers, NMR measurements of PEGDA-700, 575, 302 and 258 are performed at 111 °C.
The NMR signal decay curves have been bi-exponentially fitted and the resulting relaxation times are plotted reciprocally against the glass transition temperatures, in figure 5.10. The reciprocal values of both components of the bi-exponential T_2-fit, T_2^{short} and T_2^{long} show a linear dependence on the glass transition temperature. Because there is also a linear dependence between the glass transition temperature and the reciprocal chain length (figure 5.6), this means that the T_2 relaxation rate can be related to the chain length.
One remark concerning the measurement of PEGDA-258 has to be made. The measurements on PEGDA-302 in figure 5.9 show that the plateau of constant T_2 starts between 50 °C and 68 °C above the glass transition temperature. If the same is true for PEGDA-258 ($T_g = 64$ °C) then the plateau of constant T_2 may not have been reached at 111°C, resulting in a too low measurement of T_2. However it may be argued that in a polymer with a higher cross-link density the increase of T_2 upon heating above T_g is restricted earlier on in the heating process because of lower mobility of the shorter chains. This means that the plateau is reached at temperatures closer to T_g for PEGDA 258 than expected from the measurement of the plateau value of PEGDA-302.
A remark has to be made to the behaviour of the long T_2 component as a function of T_g. In several publications[4,21] the short T_2 component has been linked to the chains between cross-links, while the long T_2 has been linked to dangling chains, free linear chains and loops. Thus only a dependence between T_g and the short T_2 component is expected. But, as shown in figure 5.6, both components show

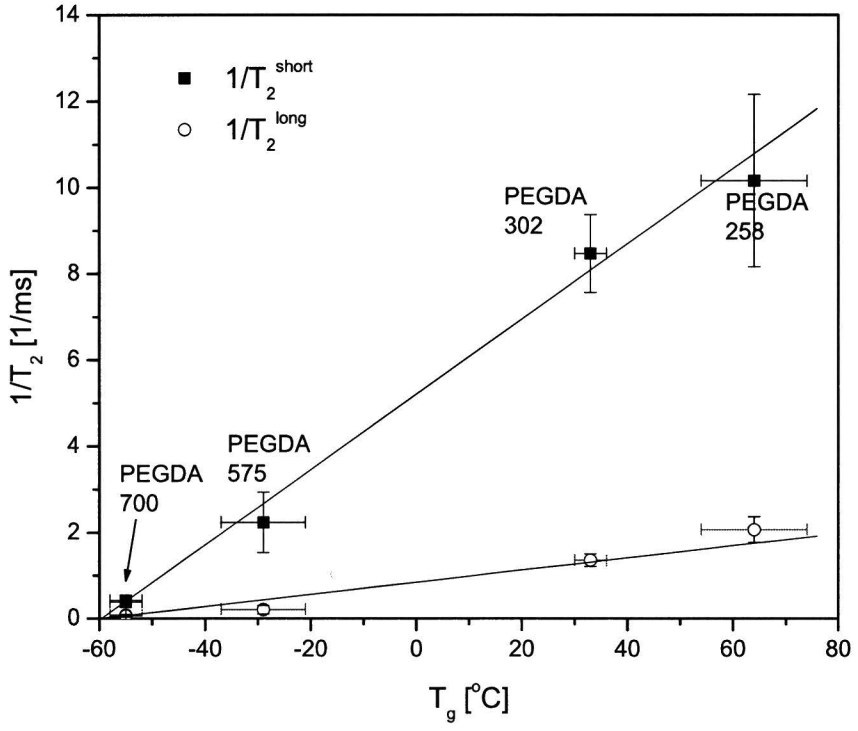

Figure 5.10: *Reciprocal values of relaxation times T_2^{long} and T_2^{short} have been plotted as a function of the glass transition temperature of various UV cured PEGDA oligomers. The relaxation times are obtained from a bi-exponential fit of the decay curves of an Ostroff-Waugh measurement with 100 μs inter echo time at a temperature of 111 °C .*

a dependence on T_g. This indicates that in the measurements both relaxation components are due to chains between cross-links. This assumption implies that no additional T_2 component due to dangling and free linear chains and loops is observed, indicating a negligible amount of these polymer structure types in the samples.

5.3 Triple layer poly-urethane coating

The results of measurements on PEGDA show a clear relation between the glass transition temperature T_g and the reciprocal relaxation time T_2. A sample with 3 different layers of polyurethane coatings presents an opportunity to investigate the possibilities for the acquisition of depth resolved information on the glass transition temperature. The composition of the sample as well as the glass transition temperatures of the layers are presented in table 5.4.

NMR measurements have been performed on this sample at various temperatures between 22 °C and 110 °C . The results of these measurements are plotted in figure 5.11. This figure only reveals significant differences between the three

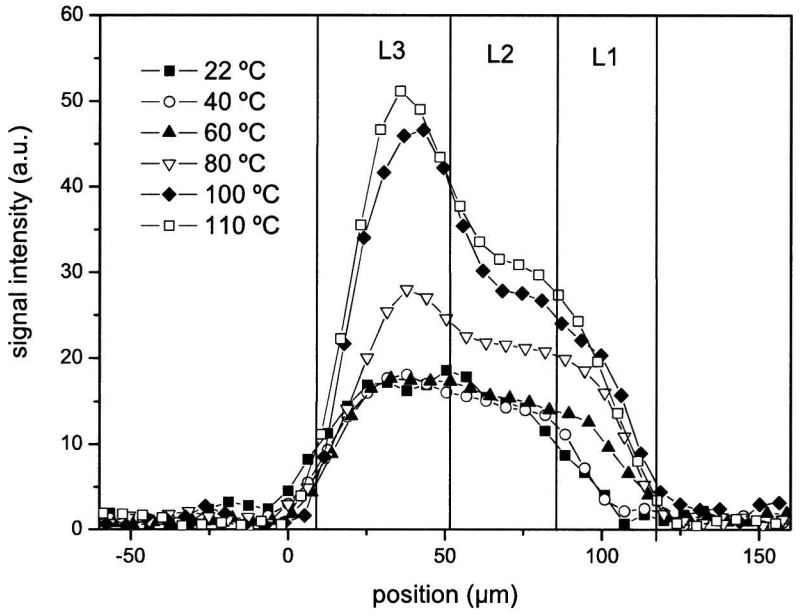

Figure 5.11: *NMR profiles of the three layer polyurethane sample, recorded at several temperatures. The top of the sample is near* 0 μm *while the bottom is near* 125 μm.

Layer	T_g [°C]	Crossl. density [mmol/cm^3]
1	79	1.58
2	69	0.98
3	61	0.12

Table 5.4: *Characteristic properties of the three-layer sample as provided by Akzo-Nobel.*

layers at temperatures above the highest glass transition temperature. The uppermost layer, layer 3 in table 5.4, starts to show a significant increase in signal intensity from 80°C. The middle layer also starts to show an increased signal-intensity, although to a lesser degree than the upper layer. At this temperature, which is approximately the glass transition temperature of layer 1, the latter layer shows a small signal whereas its signal at lower temperatures is very fast decaying ($T_2 \approx 60\ \mu$s) and barely visible.

At temperatures sufficiently far above glass transition temperature, one would expect to find a strong correlation between the glass transition temperature and T_2, see equation 3.2. This implies that the three layers should be distinguishable in a T_2-profile of the sample. Such a T_2 profile is shown in figure 5.12.

There is a distinct difference in this T_2 profile between layer 1 and layer 2. Layer 1 has much shorter T_2 components than layer 2. This difference in T_2 is qualitatively consistent with the difference in glass transition temperature, 79 °C for layer 1 versus 69 °C for layer 2. No difference in T_2 is observed between layer 2

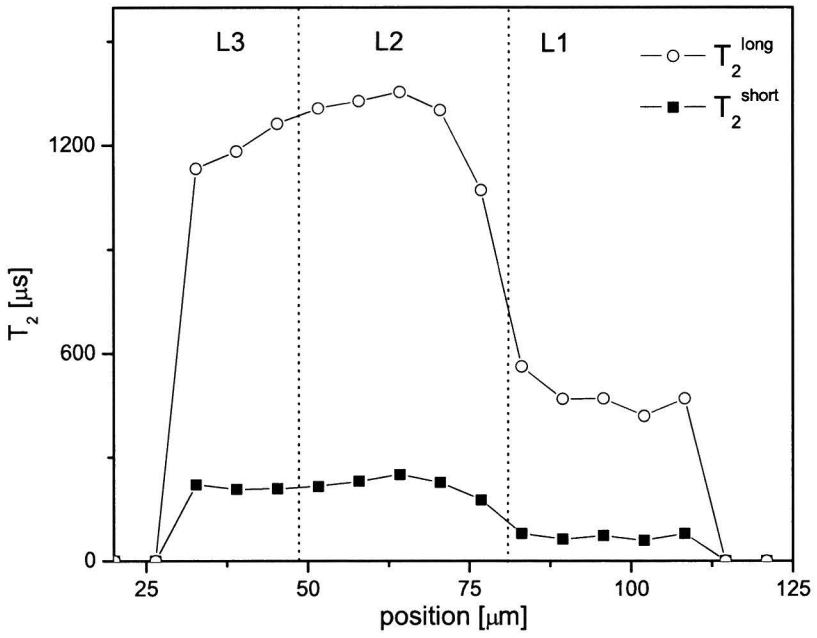

Figure 5.12: *T_2-profile of the triple layer poly-urethane sample. The data was measured at a temperature of 110 °C and the relaxation times T_2^{short} and T_2^{long} are derived from a bi-exponential fit of the signal decay.*

and 3 in figure 5.12, although there is a difference in T_g between these layers. Nevertheless, layer 2 and 3 can be distinguished by a difference in signal intensity (figure 5.11). Assuming a similar hydrogen density in both layers, this indicates the presence of a very short T_2 component in layer 2. The relaxation time of this very short T_2 component is smaller than the inter echo time and as a result the associated signal has already vanished before the first echo.

5.4 EHA

Contrary to the acrylate in the previous section (PEGDA), which forms a cross-linked network upon curing, the acrylate investigated in this section (EHA) forms branched chains. This difference in polymer structure results in more degrees of freedom and a higher mobility in the polymer, which should have a significant effect on the NMR signal. In this section the observed NMR signal decay of EHA will be presented and discussed. Also the properties of the NMR signal decay are related to the microscopic motions in the polymer.

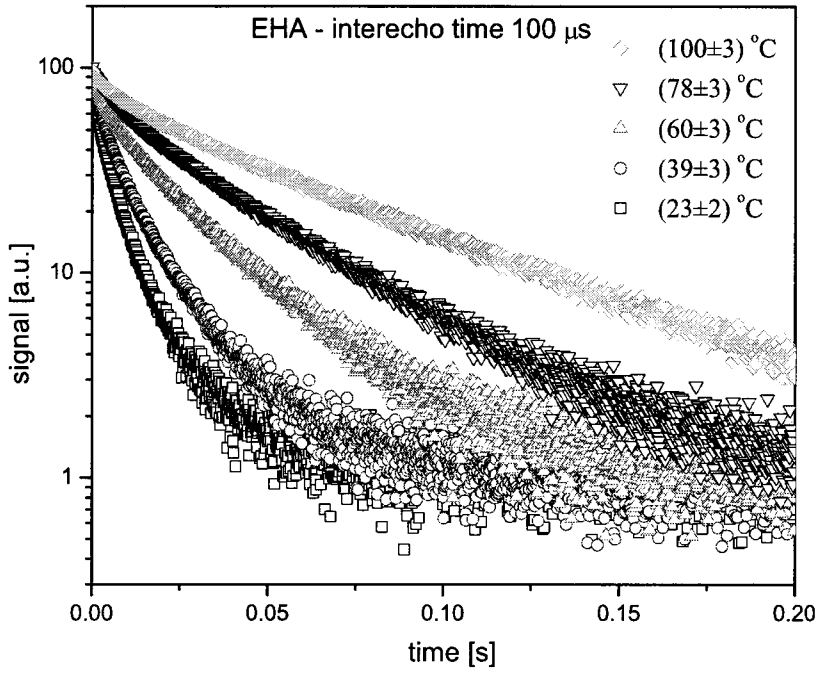

Figure 5.13: *Decay of the NMR signal of UV cured EHA at various temperatures. The signal decay is much slower than the signal decay of UV cured PEGDA (figure 5.7).*

5.4.1 Sample preparation

EHA was mixed with 1 weight-% photoinitiator (HCPK) and was applied onto glass substrates. After this, the samples were placed in a nitrogen atmosphere for approximately 15–20 minutes to minimise the dissolved oxygen. Next the samples were UV-cured for 30 seconds, also in the nitrogen atmosphere. Although the samples were created with a 200 μm spiral applicator, the resulting layers are approximately 70 μm thick. This is a result of the low viscosity of uncured EHA; it flows off the substrate before curing. The final coating is viscous and very sticky, so caution has to be paid to prevent contamination of the sample.

5.4.2 NMR signal decay of EHA

Because of the absence of a cross-linked network in UV cured EHA, the polymer chains have a higher mobility than in UV cured PEGDA. This results in a much slower decay of the NMR signal of cured EHA.
In this section the NMR signal decay of UV cured EHA is quantified in two ways. The first is by means of a bi-exponential fit. The bi-exponential fit is the best compromise between fit-stability and accurate description of the data.

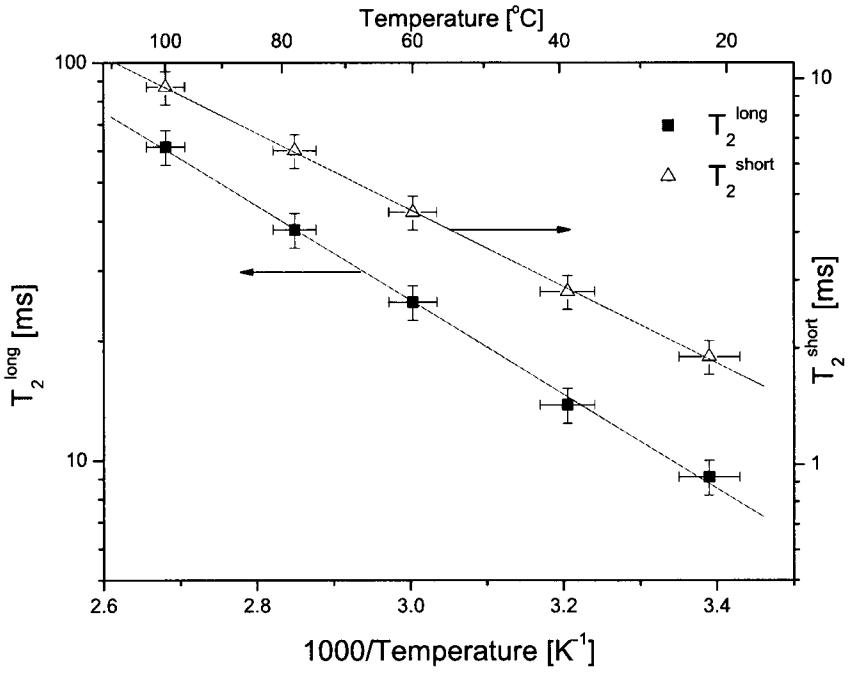

Figure 5.14: *Temperature dependence of the relaxation times derived from a bi-exponential fit of the EHA decay curves plotted in figure 5.13. Within the measured temperature range there appears to be an exponential relation between the relaxation time (T_2) and the reciprocal temperature.*

The second fitting-method is by means of a stretched exponential function

$$S = S_0 \exp\left[-\left(\frac{t}{T_2^{str}}\right)^{\beta}\right], \tag{5.5}$$

where S is the signal intensity, t the time, T_2^{str} a characteristic relaxation time and β a stretching parameter between zero and unity. This function is also known as the Kohlrausch-William-Watts (KWW) function. Although the physical processes behind this function are not fully understood[26], it is generally accepted that this function describes a wide range of experimental relaxation data, such as viscoelastic and dielectric relaxation and NMR relaxation in polymers.[27,28,29]. The stretched exponential fit was found to describe the relaxation data of cured EHA more accurately than the bi-exponential fit. Interpretation of the stretched exponential fit is, however, less straight-forward because of the lack of knowledge of the physical processes in the NMR relaxation of EHA leading to the stretched exponential decay.

Effect of temperature on the signal decay

The NMR signal of UV cured EHA is shown in figure 5.13 for several temperatures. As already mentioned above, the decay curves are fitted with a bi-exponential and

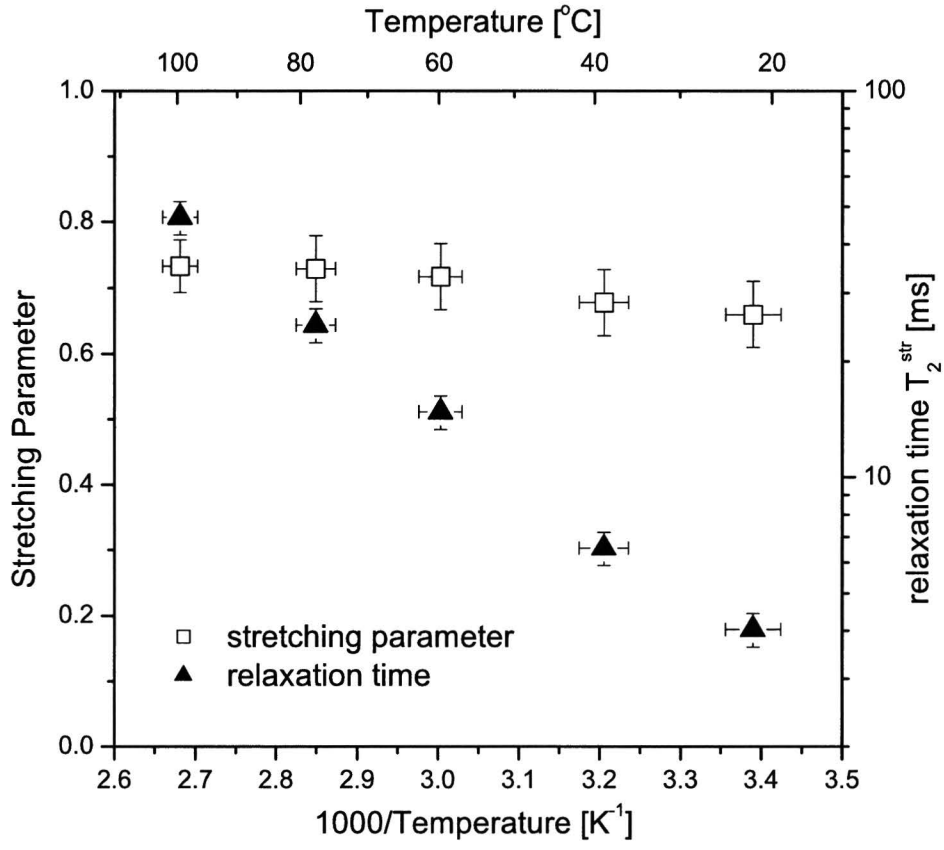

Figure 5.15: *Temperature dependence of the stretching factor β and characteristic relaxation time T_2^{str}, derived from fits of a stretched exponential function to the data on UV cured EHA, shown in figure 5.13.*

a stretched exponential function.

bi-exponential fit Both T_2-components of the bi-exponential fit (see figure 5.14) show a behaviour where $\ln(T_2)$ is inversely proportional to the temperature T. In the investigated temperature range, EHA does not show a plateau of constant T_2, like PEGDA-302 in figure 5.9. Thermal activation energies E_0 can be calculated from the slope in figure 5.14, see equation 5.4. This results in $E_0^{short}/k_B = (2.0 \pm 0.3) \times 10^3$ K for the short relaxation time and $E_0^{long}/k_B = 2.8 \pm 0.2 \times 10^3$ K for the long relaxation time.

Stretched exponential fit The relaxation time T_2^{str} and stretching parameter of the stretched exponential fit are shown in figure 5.15. T_2^{str} shows an exponential dependence on the reciprocal temperature, similar to the one found for the bi-exponential fit. The slope of $\ln(T_2)$ versus T^{-1} results in $E_{0,str}/k_B = (3.4 \pm 0.2) \times 10^3$ K. The stretching parameter β does not change significantly between 22 °C

and 100 °C.

Discussion With both fitting procedures an exponential dependence of the relaxation times T_2^{short} and T_2^{long}, respectively T_2^{str}, on the reciprocal temperature (T^{-1}) is found. No plateau of constant T_2 is observed. This is consistent with the absence of a cross-linked network in cured EHA. Only cross-linked networks are expected to show such a plateau, see section 3.3.
The linear relation between $\ln(T_2)$ and T^{-1} of T_2^{short} and T_2^{long}, respectively T_2^{str}, suggests a thermal activation of the motions of the polymer chains. The energy derived from the slope of $\ln(T_2)$ vs T^{-1} or $\ln(T_2^{str})$ vs T^{-1} can be viewed as an energy barrier for certain motions in the polymer.
The activation energies derived from the bi and stretched exponential fits of the NMR signal decay of EHA are within the same order of magnitude as the activation energy derived for PEGDA (section 5.2.4). The energy derived from the stretched-exponential fit is higher than the energies derived from the both components of the bi-exponential fit. Because of a higher fitting stability of the stretched exponential function compared to the bi-exponential fit, the value for E_0 found using the stretched exponential fit is likely to be more reliable.
The linear dependence of $\ln(T_2^{short})$, $\ln(T_2^{long})$, and $\ln(T_2^{str})$ on T^{-1} is an indication that the degrees of freedom for motions responsible for the relaxation do not change as a function of temperature. A change in degrees of freedom of the motions is likely to change the activation energies associated with the processes, resulting in a change of the slope of T_2^{str} vs T^{-1}. This means that the averaging of the dipole-dipole interactions is dominated by the same type of motion (or component of the polymer) in the whole temperature range. Only the intensity of the motion and thus the degree of averaging of the dipole-interactions increases with increasing temperature.

Dependence of the relaxation on the inter echo time

Measurements on cured EHA show a dependence of the signal decay on the inter echo time. This is illustrated by, for example, the decay curves plotted with filled symbols in figure 5.16. It has found to be possible to apply a scaling factor to the time: $t \rightarrow t \cdot t_{echo}^{\gamma}$, so that the data for the various inter echo times collapses onto a single curve.
Application of this scaling factor (see for example figure 5.16) shows that $\gamma = 0.21 \pm 0.03$. Additional measurements revealed that γ is constant for all temperatures, and all used field strengths (0.3 T, 0.7 T, 1.5 T and 4.7 T.) The same inter echo time dependent behaviour with the same scaling factor is observed in measurements with CPMG sequences.

Possible explanations for the inter echo time dependence of the relaxation time

There are several possible explanations for an inter echo time dependence of the NMR signal decay. The most common is diffusion of chains and chain segments

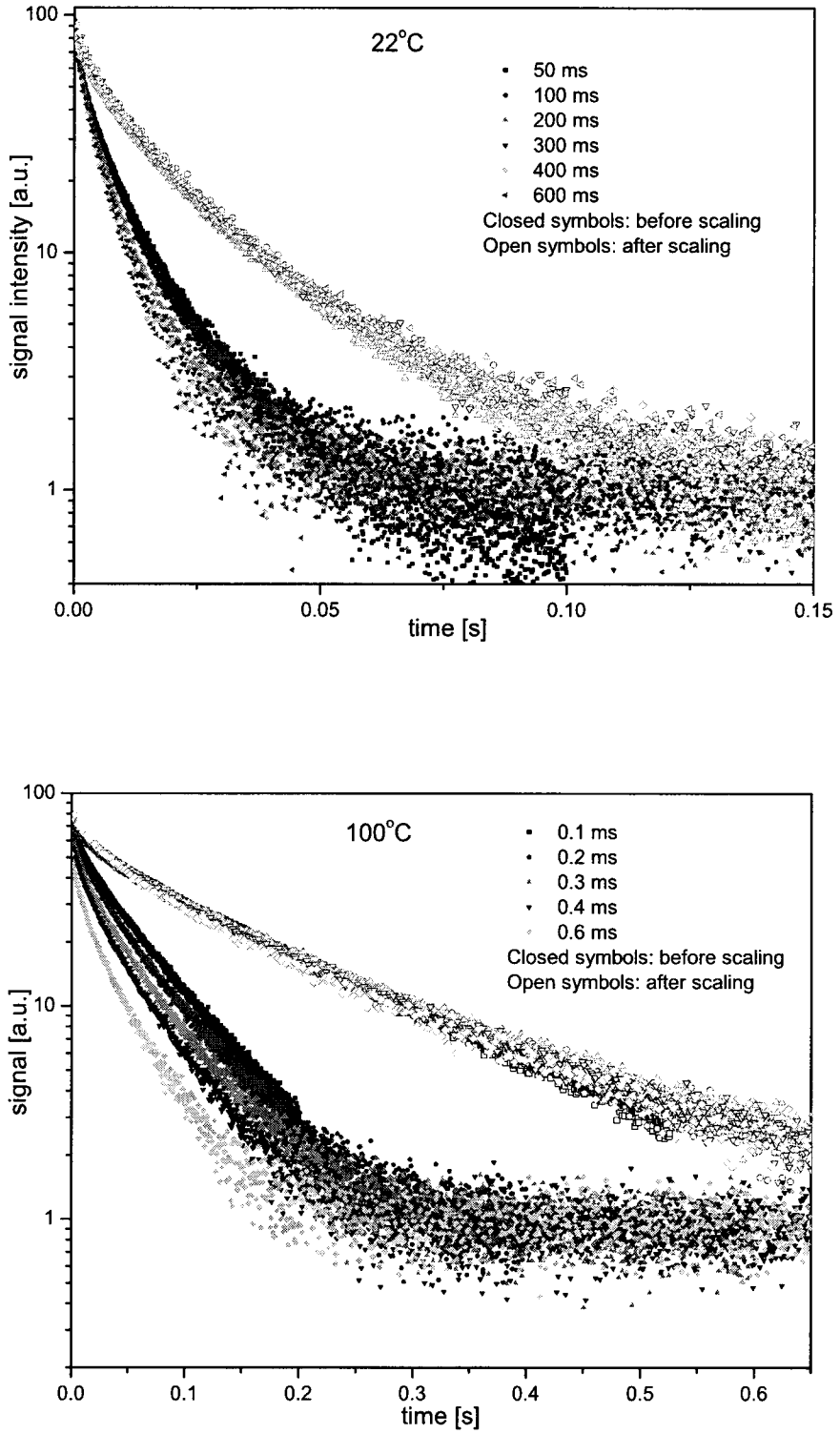

Figure 5.16: *NMR signal decay of EHA measured with an OW sequence at 22 °C (top) and 100 °C (bottom.) The filled symbols represent the original decay, whereas the open symbols show the decay with the original time multiplied by a factor* $(t_{echo}/[\mu s])^{0.21}$.

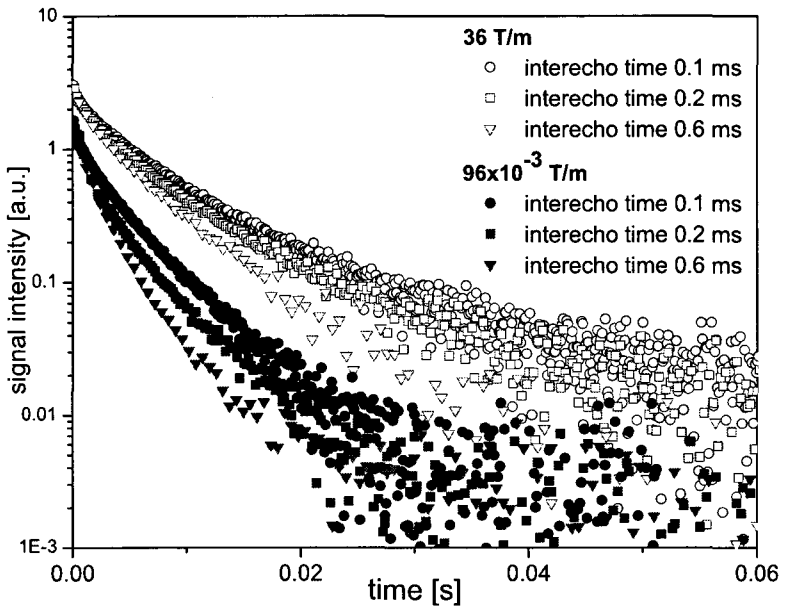

Figure 5.17: *NMR signal decay (Ostroff-Waugh) of EHA measured with a gradient of 36.4 T/m and a much smaller gradient of 96 mT/m for various inter echo times.*

in an external magnetic field gradient, but there are also other possibilities like spin diffusion, spin locking and subsequent measurement of T_1^ρ, and dipole-dipole interactions with long correlation times. These possible explanations will now be subsequently investigated.

Diffusion Usually a dependence of the NMR signal decay on the inter echo time is explained by diffusion of chains or chain segments in a gradient of the B_0 field. According to equation 2.18 and appendix A, ordinary diffusion should result in a quadratic dependence of the NMR signal decay on the inter echo time: $\gamma = 2$. This is not the case in the measurements on cured EHA, where $\gamma = 0.21 \pm 0.03$. A possible explanation for the non-quadratic dependence of the NMR signal decay on the inter echo time might be anomalous diffusion. Anomalous diffusion is frequently reported[29] in polymers and exhibits relatively large diffusion coefficients on short time scales and smaller diffusion coefficients on longer time scales. The displacement r by anomalous diffusion is described by $< r^2 >= Dt^\alpha$ with D the diffusion coefficient, t the time and $0 < a < 1$. This kind of diffusion results in $0 < \gamma < 2$.
A non-quadratic dependence of the relaxation on the inter echo time is also found for flip-flop spin diffusion[29,30,31]. Flip-flop spin diffusion is a displacement of spin polarisation by mutual flipping of coupled pairs of dipoles along the polymer chain. One spin changes its state from up to down, while the partner spin changes its state in the opposite direction. Subsequent spin flip-flopping along a chain can results in a displacement of spin polarisation in an equivalent way as the displace-

ment of spins by diffusion of chains or chain segments. Spin diffusion is known to exhibit diffusion coefficients in the order of 10^{-16} m^2/s.
However, for any kind of diffusion (normal, anomalous, or spin diffusion) in an external field gradient, the effect of the diffusion on the relaxation has to be dependent on the magnetic field gradient (see for example equation 2.18). This has been checked by measurements with a gradient of 36.4 T/m and 96 mT/m. The results of these measurements are shown in figure 5.17. Although a gradient of 96 mT/m is almost negligible compared to a gradient of 36.4 T/m, a similar inter echo time dependence of the relaxation is observed in both measurements. Therefore diffusion can not be responsible for the observed inter echo time dependence of the signal decay. The dependence has to be explained by another mechanism.

$T_{1,\rho}$ In the limit of a continuous RF-field the magnetisation in the rotating frame of reference will process around the $\vec{B_1}$ field. The magnetisation in the rotating frame of reference along $\vec{B_1}$ will decay with a characteristic time scale $T_{1,\rho}$, see Slichter[32]. When going from a long inter echo time to a shorter inter echo time the duty cycle increases. In the limit of very high duty cycles $T_{1,\rho}$ is measured instead of T_2, which might account for the observed increase of the measured T_2 for short inter echo times. However, even with an inter echo time of 50 μs on the 1.5 T, 36.4 T/m setup the duty cycle during the pulse sequence is just 2%, so it is unlikely that the observed increase in T_2 is due to a locking of the spins along the $\vec{B_1}$ field.

Residual dipolar coupling In polymer systems, molecular motions tend to be strongly anisotropic: for example, reorientations around the chain axis are much faster than reorientations of the chain axis itself. Usually in NMR theory a complete motional averaging of all local fields resulting from dipolar interactions is assumed. In case of strongly anisotropic motions, part of the local fields may not have been averaged to zero on the time scale of the NMR experiment, resulting in a residual dipolar coupling. Several publications[33,34,35] report such a residual dipolar coupling in polymer systems.
If motions responsible for averaging of these residual dipolar couplings have characteristic time scales in the order of the inter echo time, it is possible that a variation of the inter echo time results in a variation of the residual dipolar coupling. This might result in the observed dependence of T_2 on t_{echo}.
An indication for interactions on longer characteristic time scales is provided by a measurement with a stimulated echo sequence (section 2.2.4). The ratio between the signal intensity of the stimulated echo and the solid echo S_{stim}/S_{sol} as a function of τ_2 is shown in figure 5.18. After an initial relatively fast decay, the ratio S_{stim}/S_{sol} decreases with the longitudinal relaxation time T_1 on a longer time scale.
Because the longitudinal relaxation dominates the decay in figure 5.18 but is not of primary interest, S_{stim}/S_{sol} was compensated for the longitudinal relaxation. A plot of S_{stim}/S_{sol} versus τ_2, which is compensated for longitudinal relaxation, is shown in figure 5.19. The initial decay of the data in figure 5.19 can be charac-

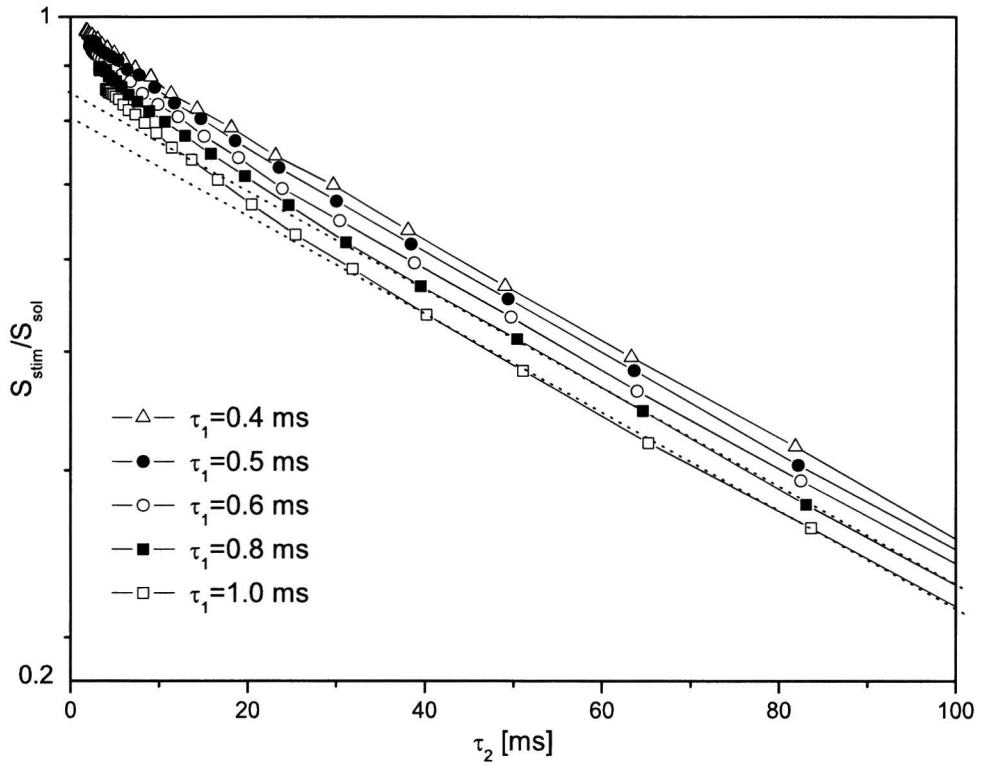

Figure 5.18: *Stimulated echo measurement of EHA at room temperature. The ratio between the signal intensities of the stimulated and solid echo is plotted against the time τ_2 between the second and third 90° pulse. The different lines refer to different τ_1 values, the time between the first and second 90°. The two dotted lines indicate the longitudinal relaxation.*

terised with a characteristic time scale by fitting with the equation:

$$\frac{S_{stim}}{S_{sol}\ \exp(-\tau_2/T_1)} = \exp\left(-\frac{\tau_2}{\tau_c}\right) + C_0\ , \tag{5.6}$$

where C_0 is the asymptotic value at high τ_2 values and τ_c a characteristic time scale for the initial decay. Performing such a fit reveals that $\tau_c = (23 \pm 5)$ ms at room temperature (ca. 24 °C) with no clear dependence on τ_1.
Measurements at higher temperatures show a strong decrease of τ_c with increasing temperature. At 54 °C , $\tau_c = (5 \pm 4)$ms, whereas at higher temperatures τ_c becomes too short to be measured.

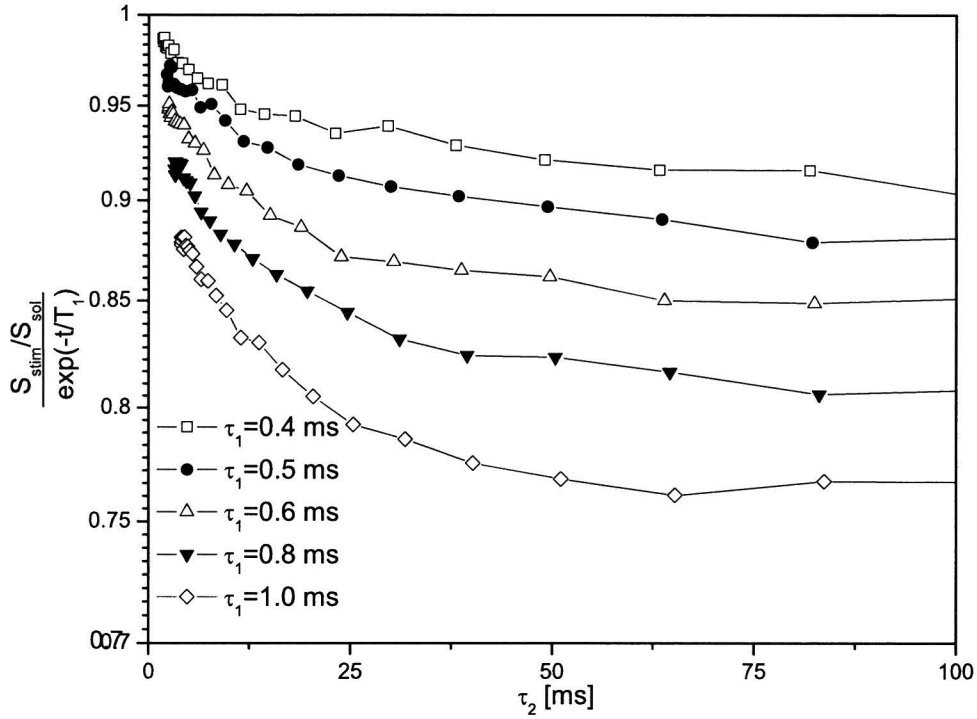

Figure 5.19: *Stimulated echo measurement of EHA at room temperature. The data in this figure is identical to the data in figure 5.18, but the ratios of the signal intensities of the stimulated and solid echo have been compensated for longitudinal relaxation.*

Chapter 6

Conclusions and recommendations

In chapter 5, NMR measurements on UV cured acrylates were presented and discussed. The most important conclusions, recommendations, and opportunities for future research will be presented and discussed in this chapter. First, the conclusions concerning the investigation of the properties of the polymer structure by analysis of the transverse relaxation time are presented. Next, the conclusions concerning the investigation of microscopic motions in the polymer by the NMR signal decay are presented and discussed.
Many measurements in this report were performed at elevated temperatures. Therefore, at the end of this chapter some practical aspects of the additional sample heating equipment (section 2.3.1) and requirements for an improved setup will be discussed.

6.1 Relation between glass transition temperature and T_2

A relation between the glass transition temperature and the transverse relaxation for cured PEGDA has been experimentally confirmed. The relation between the glass transition temperature T_g and the transverse relaxation time is in agreement with the findings by Litvinov and Dias[4]. Also a linear relation between the chain length M_c and T_g as predicted by formula 3.1 has been shown, hence T_2 can also be linked to M_c. Assuming the relation between the cross-link density ρ_c and M_c^{-1} to be linear, the results are also in agreement with the prediction[19,20] $T_2 \propto \rho_c^{-1}$.
NMR measurements on a triple layer polyurethane coating show that investigation of polymer structure properties like T_g by measuring T_2 is not always straightforward. In the measurements on the polyurethane sample, T_2 was not sufficiently large to distinguish all layers from each other. To distinguish the layers, the signal intensity had to be taken into account. The difference in signal intensity is probably due to very short T_2 components, which cannot be measured with the used inter echo time setting. Although the inter echo time settings can be adjusted to recover at least part of the signal of these short T_2 components, this

deteriorates the resolution. Coatings with high cross-link densities will have short transverse relaxation times, so a spatially resolved investigation of the properties of a polymer structure in highly cross-linked coatings demands a compromise between spatial resolution and the ability to distinguish short T_2 values.

6.2 Information on microscopic motions and interactions

The characteristics of the NMR signal decay as a function of temperature were investigated for cured EHA and cured PEGDA. The thermal activation energies associated with the increase in T_2 in PEGDA ($E_0/k_B \sim 10^3$ K) and EHA ($E_0/k_B = (3.4 \pm 0.2) \times 10^3$ K) are in the same order of magnitude, which is an indication that the averaging of dipolar interactions is governed by similar types of motions (e.g. segmental or chain motions) in both polymer systems.
In case of PEGDA-302, T_2 reached a constant value at temperatures approximately 60 °C above glass transition temperature. Such a constant T_2 was not observed in EHA, even at temperatures far above glass transition temperature. This is in agreement with the theory suggested by Gotlib et al.[19], who suggests that part of the dipolar interactions are not averaged to zero in cross-linked networks, because of the anisotropic motions resulting from restrictions imposed by the fixed cross-links, see for more detail section 3.3. In branched chains like in cured EHA there exist no such fixed cross-links and consequently upon heating all dipolar interactions will eventually be averaged to zero. However, a complete averaging may only take place on long time scales. At short time scales motions in EHA are still anisotropic, resulting in residual dipolar interactions, which depend on the experimental time scale. At long time scales the residual dipolar interactions are averaged to zero. This time scale dependent anisotropy of the motional averaging of the dipolar interactions may be associated with observed inter echo time dependence of the NMR signal in EHA, but the exact mechanism is not clear yet.

6.3 Sample heating equipment

Two ways of heating were distinguished in this report: Heating by RF-pulses and heating by the sample heating equipment (section 2.3.1).
The heating by RF pulses should always be kept constant in T_2 measurements. This can be achieved by adjusting the long delay, so that the average number of pulses per second remains constant.
The heating equipment can serve two purposes: to raise the temperature of the sample sufficiently far above the glass transition temperature, where T_2 becomes a function of ρ_c, and, second, to investigate the NMR signal as a function temperature. In the first case, investigation of T_2 as a function of cross-link density, measurements have to be performed in the temperature range of constant T_2. Consequently, temperature variations of several degrees do not change the mea-

sured T_2 value and temperature stability is not an important issue.
In the second case, measurement of the behaviour of the NMR signal as a function of temperature (e.g. figure 5.9), the accuracy and stability of the current heating equipment is more important. During a measurement of 2 hours, temperature fluctuations of 4 °C have been observed. This means that for a more detailed investigation of the NMR signal as a function of temperature, the heating equipment has to be improved. A higher stability of the temperature is recommended.

Appendix A

Comparison between OW and CPMG signal decay

Measurements performed on NMR-setups with high field-gradients involve some additional requirements regarding the pulse sequences. One issue is the area excited by 90° and 180° pulses. A 180° pulse will only excite half the area excited by a 90° pulse because of a smaller frequency spectrum of the 180° pulse. To excite the same area by each pulse, an Ostroff-Waugh (OW) sequence, containing only 90° pulses, can be used. Because only 90° pulses are used, every pulse excites the same area.
Although the CPMG sequence and the OW sequence are largely similar, there are some differences between the two which we will discuss in this appendix.

A.1 Echo intensity

One property of the OW sequence is a variation in spin-echo intensity. The amplitude of the first echo of an OW sequence is just 1/2 of the magnitude of to the first echo of a CPMG sequence. Although the first echo shows the largest difference in intensity, the following echoes also show a variation in signal intensity, see for example figure A.2. The values of the intensities of the echoes can be obtained by calculation of the coherent pathways[36]. This results in a behaviour where pairs of successive echoes have the same intensity, see table A.1 and figure A.1. The value of the echo intensity converges to $\frac{1}{2}\sqrt{2}$. The values in A.1 can be used to correct the OW-decay before further analysis and interpretation of the data.
In many cases a correction of only the first echo by 3/2 is sufficient. This correction makes the intensity of the first echo equal to the intensity of the second echo. Correction values for other echoes are neglected, because the experimental error is often larger than the variation in echo intensity.

echo number	intensity
1	1/2
2 and 3	3/4
4 and 5	11/16
6 and 7	46/64
8 and 9	179/256
10 and 11	730/1024
etc.	

Table A.1: *Magnitude of the OW-echoes, compared to the magnitude of the corresponding CPMG-echoes. The values correspond to the data shown in figure A.1.*

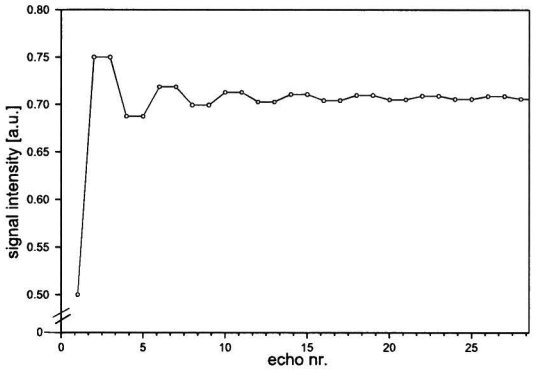

Figure A.1: *Simulation with $T_2 = T_1 = \infty$. The ratio between the echo intensity of an OW sequence and the corresponding echo intensity of a CPMG sequence as a function of the echo number is shown.*

A.2 T_2 effects

The measured T_2 relaxation time with an OW sequence is longer then when measured with CPMG sequence, which can be observed in the decay curve of both sequences, see figure A.2. As a result of the 90°-pulses, part of the longitudinal magnetisation (M_z) is transferred to the transverse magnetisation ($M_{x,y}$). The longitudinal magnetisation decays with the T_1 relaxation time, which is higher than T_2, resulting in a slower signal decay.
The difference in the measured (effective) T_2 in both sequences depends on the ratio T_2/T_1. In figure A.3 the ratio T_2^{OW}/T_1 of an OW sequence is shown as a function of T_2^{CPMG}/T_1 of a CPMG sequence.

A.3 Influence of diffusion

The effect of diffusion is different in measurements with OW and CPMG sequences. To quantify the effect, a simulation of OW and CPMG sequences is performed. In this simulation the complete signal decay is due to diffusion with a diffusion coefficient of $2.1 \times 10^{-9}\mathrm{m}^2/\mathrm{s}$ in a gradient of 36.4 T/m. Transverse and longitudinal relaxation are disabled in the simulation, and the simulation is performed with inter echo time settings of 50, 100, 200, 300, and 400 μs
The decay curves from the simulation with an inter echo time of 100 μs are plotted in figure A.4. The signal of the OW sequence shows a faster decay than the signal of the CPMG sequence. A linear dependence of the reciprocal signal decay rate on the squared inter echo time t_{echo}^2 is observed in the simulations of both the OW and the CPMG sequences (see figure A.5). The simulation of the CPMG sequence is in agreement with equation 2.18. For the OW sequence, the simulations indicate that the constant of 1/12 in equation 2.18, has to be substituted by 1/6.0.
The increase of this constant in equation 2.18 for an OW sequence can be un-

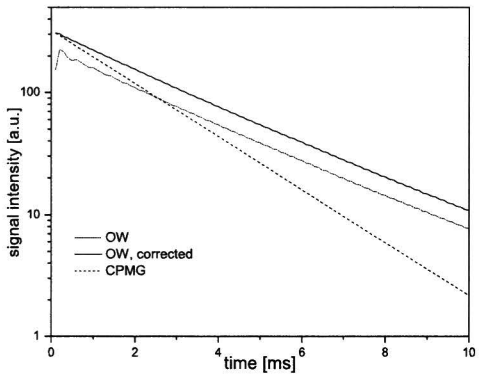

Figure A.2: *Decay curve of OW and CPMG sequences, simulated without the influence of diffusion. Shown are the signal of a CPMG sequence, and that of an OW sequence before and after correction according to table A.1.*

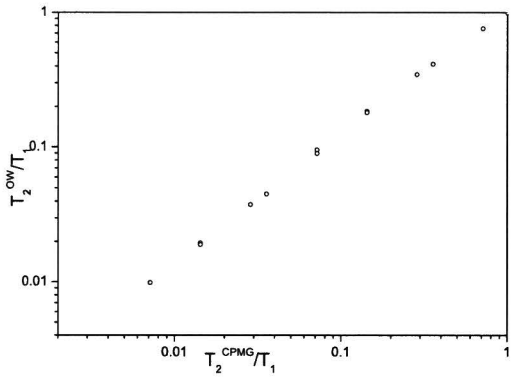

Figure A.3: *Ratio T_2/T_1 measured with an OW sequence, as a function of the T_2/T_1 ratio measured with a CPMG sequence. The data points are obtained from simulations of both sequences.*

derstood from the fact that the OW sequence consists of 90° pulses, whereas the CPMG sequence consists of 180° pulses. During an OW sequence, the spin rephase less often than during a CPMG sequence, thereby increasing the amount of dephasing due to diffusion before rephasing, increasing the constant in equation 2.18.

A.4 Deviation of the pulse-length

In NMR experiments the flip angle of a 90° or 180° pulse often deviates from the ideal values of 90° or 180°. This can be due to inaccurate pulse settings or to a variation of the RF field strength as a function of distance to the NMR coil.
To gain insight into the errors caused by an incorrect flip angle, measurements and simulations were performed with varying flip angles in CPMG and OW sequences. In case of the CPMG sequence the 180° pulse is assumed to be twice the duration of the 90° pulse.
The measurements were performed on a piece of rubber with $T_1 = 0.6$ s and $T_2 = 45$ ms. These values were also used as input values for the simulation. The results are presented in figure A.6. The measurements and simulations of the CPMG sequence show a parabolic variation of the decay rate around the optimum flip angle of 180°. The OW sequence shows both in the measurement and the simulation roughly a linear variation of the decay rate as a function of the flip angle.
The effective T_2 values derived from the measurements are longer than the simulated values. This may be caused by a second, very long T_1 component (> 1 s) which was present in the measurement on the rubber sample, but which was neglected in the simulation.

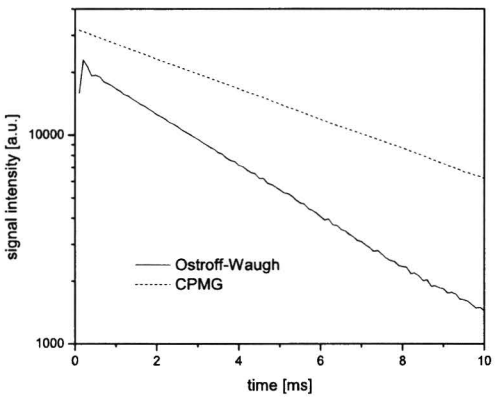

Figure A.4: *Signal intensity as a function of time of an simulated Ostroff-Waugh and a CPMG sequence due to diffusion. The inter echo time is* 100 μs

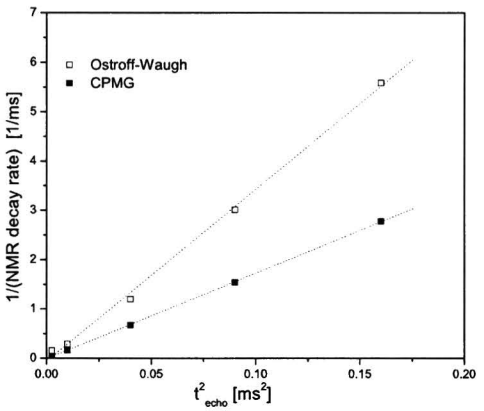

Figure A.5: *The reciprocal NMR signal decay rate versus the squared inter echo time for both OW and CPMG sequences.*

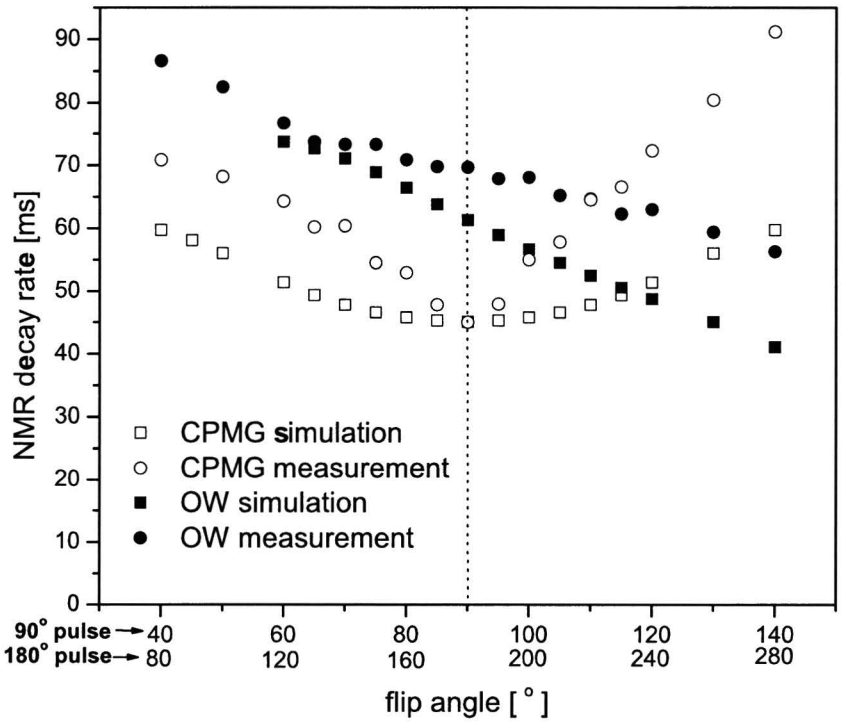

Figure A.6: *Decay rate as a function of the the flip angle of the* 90° *and* 180° *pulses. Data obtained from both measurements and simulation are shown. The values on the horizontal axis show the flip angle of the* 90° *pulse (top) and that of the* 180° *pulse (bottom). Data from simulations and measurements of a CPMG and OW sequence are shown.*

Appendix B

Resolution of the 36.4 T/m NMR setup

The maximum achievable resolution has been calculated as a function of several factors: the duration of the signal acquisition window, and the sample dependent transverse relaxation time T_2, see figure B.1. For the calculation, equations 2.14, and 2.16 are used. In the plots in figure B.1, only a limitation of the resolution by the plotted parameter is considered.
The resolution is shown within the range of 1 μm to 50 μm, because this covers most of the situations encountered during the measurements. Although a resolution of less than 1 μm seems possible, it is very hard to place a sample precise enough in respect to the field-gradient to exploit this resolution.
In liquids the limitation of the resolution is often dominated by diffusive broadening of the line width because T_2 is long and the atoms are relatively mobile, having a large diffusion coefficient D. Furthermore, the root-mean-square (RMS) displacement $\sqrt{< r^2 >} = \sqrt{6DT}$ of atoms during the experimental period T, can limit the maximum achievable resolution in liquids. However, in solid systems like coatings, D is generally very small[a], and T_2 short, so a significant influence of diffusion on the resolution is not expected[7,37].

[a] $D \approx 10^{-15}$ m^2/s for a typical polymer melt[7]

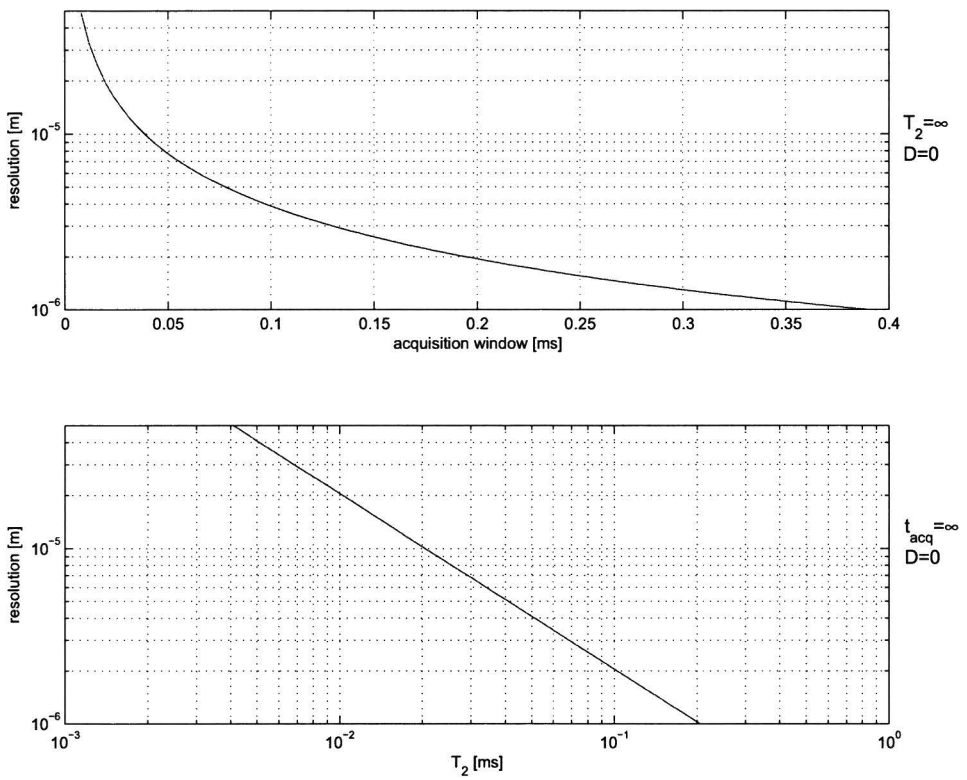

Figure B.1: *Influence of the duration of the acquisition window, and T_2, on the best achievable resolution of the* 36.4 T/m *NMR setup.*

Dankwoord

Tijdens het afstuderen ben ik in contact gekomen met veel mensen, die op de een af andere manier een bijdrage geleverd hebben. De een op wetenschappelijk gebied, de ander door emotionele steun, of een willekeurige combinatie van beiden. Alhoewel ik bij het schrijven van dit dankwoord, vast en zeker, de nodige mensen te kort doe door ze te vergeten, wil ik toch een aantal noemen.
Ten eerste uiteraard mijn begeleider *Bart Erich*, zonder wie er niet veel van dit onderzoek terecht zou zijn gekomen. Alhoewel er af en toe van die momenten waren waarop ik, een over het algemeen vredelievend en pacifistisch persoon, ernstige moordneigingen kreeg (het zal bij Bart vast niet anders geweest zijn), was het toch vooral een heel erg plezierige en constructieve samenwerking.
Verder is er *Henk Huinink*, zonder wiens theoretische benadering van allerlei NMR- en polymeerproblemen, nog minder begrepen zou zijn. *Klaas Kopinga* heeft uiteraard ook zijn steentje bijgedragen, zowel met hulp bij NMR problemen, als ook met het kritisch doorlezen van mijn verslag. *Hans Dalderop* verdient een speciale vermelding voor alle kleine en grote probleempjes die hij gedurende mijn afstudeeronderzoek voor mij heeft opgelost.
Aan de scheikundige kant van het onderzoek, wil ik graag *José Brokken* bedanken voor haar advies en ideeën op polymeergebied. Ook bij de faculteit scheikunde, wil ik *Francesca Scaltro* bedanken voor haar hulp met UV curen en het schoonmaakprocédé voor de preparaatglaasjes.
Dan komen we langzamerhand aan bij de categorie mentale steun oftewel 'geestelijke hulpverlening.' Hierin ten eerste *Leo Pel*, zonder wiens (de/con)structieve opmerkingen mijn afstudeerperiode waarschijnlijk nooit het zelfde was geweest. Leo wil ik ook bedanken voor zijn kritische observaties met betrekking tot lunchtijd. Nothing beats a Leo met een knalrode boterhamtrommel.
In de categorie Nb2.07 bewoners wil ik *Gijs van der Heijden* bedanken voor af en toe een aanvulling op een zwart gat in mijn fysica kennis.
Last but not least wil ik geen persoon, maar een waar instituut bedanken: *S.V.T.N. J.D. v.d. Waals*. Dankzij deze, was er zelfs op de donkerste momenten van mijn studie, een lichtpuntje te vinden. Op donderdag middag, ergens in de verste uithoek van de g-vleugel van N-laag!

Bibliography

[1] A. R. Marrion, editor. *The Chemistry and Physics of Coatings.* Royal Society of Chemistry, Cambridge, 1994.

[2] M. E. Nichols, C. M. Seubert, W. H. Weber, and J. L. Gerlock. A simple raman technique to measure the degree of cure in UV curable coatings. *Progress in Organic Coatings*, 43(4):226–232, 2001.

[3] A. Priola, G. Gozzelino, F. Ferrero, and G. Malucelli. Properties of polymeric films obtained from UV cured poly(ethylene glycol) diacrylates. *Polymer*, 34 (17):3653–3657, 1993.

[4] V. M. Litvinov and A. A. Dias. Analysis of network structure of UV-cured acrylates by H-1 NMR relaxation, C-13 NMR spectroscopy, and dynamic mechanical experiments. *Macromolecules*, 34(12):4051–4060, 2001.

[5] F. Bloch. Nuclear induction. *Physical Review*, 70(7-8):460–474, 1946.

[6] E. M. Purcell, H. C. Torrey, and R. V. Pound. Resonance absorption by nuclear magnetic moments in a solid. *Physical Review*, 69(1-2):37–38, 1946.

[7] P. J. McDonald and B. Newling. Stray field magnetic resonance imaging. *Reports on Progress in Physics*, 61(11):1441–1493, 1998.

[8] P.T. Callaghan. *Principles of Nuclear Resonance Microscopy.* Oxford Science Publications, 1st edition, 1991. ISBN 0-19-853997-5.

[9] E. D. Ostroff and J. S. Waugh. Multiple spin echoes and spin locking in solids. *Physical Review Letters*, 16:1097, 1966.

[10] J. S. Waugh and C. H. Wang. Multiple spin echoes in dipolar solids. *Physical Review*, 162(2):209, 1967.

[11] S.J.F. Erich. A dedicated NMR setup for 3D drying experiments. Master's thesis, TU/e, 2002.

[12] J.J. van der Sande, L.A. Rijniers, R.N.P. Meerman, and S.J.F. Erich. Programmers reference to the NMR measurement system. 2004.

[13] B. De Ruiter and R. M. Meertens. UV-curing in oxygen deficient conditions. *Macromol. Symp.*, 187:407–416, 2002.

[14] K Studer, C Decker, E Beck, and R Schwalm. Overcoming oxygen inhibition in UV-curing of acrylate coatings by carbon dioxide inerting, part I. *Progress in Organic Coatings*, 48:92–100, 2003.

[15] A. K. v. d. Vegt. *From Polymers to Plastics.* Delft University Press, Delft, 2002.

[16] T. G. Fox and S. Loshaek. Influence of molecular weight and degree of crosslinking on the specific volume and glass temperature of polymers. *Journal of Polymer Science*, 15:371–290, 1955.

[17] S. Loshaek. Crosslinked polymers. II. glass temperature of copolymers of methyl methacrylate and glycol dimethacrylates. *Journal of Polymer Science*, 15:391–404, 1955.

[18] L. E. Nielsen. *Mechanical Properties of Polymers and Composites*, volume 1. Marcel Dekker, inc., New York, 1974.

[19] Yu. Ya. Gotlib, M. I. Lifshits, V. A. Shevelev, I. S. Lishanskii, and I. V. Balanina. The influence of the chemical crosslinking network on the spin-spin relaxation of crosslinked and swelling polymer systems. *Polym. Sc. USSR (Engl. Transl.)*, 18:2630, 1976.

[20] C. G. Fry and A. C. Lind. Determination of cross-linkdensity in thermoset polymers by use of solid-state H-1-NMR techniques. *Macromolecules*, 21(5): 1292–1297, 1988.

[21] G. Simon, K. Baumann, and W. Gronski. Mc determination and molecular-dynamics in cross-linked 1,4-cis-polybutadiene - a comparison of transversal H-1-NMR and H-2-NMR relaxation. *Macromolecules*, 25(14):3624–3628, 1992.

[22] P. W. Atkins. *Physical Chemistry.* Oxford University Press, Oxford, 6 edition, 1978.

[23] R. A. Nyquist. *Interpreting Infrared, Raman and Nuclear Magnetic Resonance Spectra*, volume 1. Academic Press, San Diego, 1 edition, 2001.

[24] S. L. Boersma. New apparatus for differential thermal analysis. *Journal of the American Ceramic Society*, 38:481–484, 1955.

[25] J. Brandrup and E. H. Immergut. *Polymer Handbook.* Wiley-Interscience, London, 3rd edition, 1989.

[26] D. Apitz and P. M. Johansen. Limitations of the stretched exponential function for describing dynamics in disordered solid materials. *Journal of Applied Physics*, 97(6), 2005.

[27] R. G. Palmer, D. L. Stein, E. Abrahams, and P. W. Anderson. Models of hierarchically constrained dynamics for glassy relaxation. *Physical Review Letters*, 53(10):958–961, 1984.

[28] J. C. Phillips and J. M. Vandenberg. Subensembles and kohlrausch relaxation in electronic and molecular glasses. *Journal of Physics-Condensed Matter*, 9 (18):L251–L258, 1997.

[29] R. Kimmich and N. Fatkullin. Polymer chain dynamics and NMR. *NMR - 3D Analysis - Photopolymerization*, 170:1–113, 2004.

[30] E. Fischer, R. Kimmich, and N. Fatkullin. Spin diffusion in melts of entangled polymers. *Journal of Chemical Physics*, 106(23):9883–9888, 1997.

[31] E. Fischer, R. Kimmich, N. Fatkullin, and G. Yatsenko. Segment diffusion and flip-flop spin diffusion in entangled polyethyleneoxide melts: A field-gradient nmr diffusometry study. *Physical Review e*, 62(1):775–782, 2000.

[32] C. P. Slichter. *Principles of Magnetic Resonance.* Springer, Berlin, 3 edition, 1990.

[33] R. C. Ball, P. T. Callaghan, and E. T. Samulski. A simplified approach to the interpretation of nuclear spin correlations in entangled polymeric liquids. *Journal of Chemical Physics*, 106(17):7352–7361, 1997.

[34] E. Fischer, F. Grinberg, R. Kimmich, and S. Hafner. Characterization of polymer networks using the dipolar correlation effect on the stimulated echo and field-cycling nuclear-magnetic resonance relaxometry. *Journal of Chemical Physics*, 109(2):846–854, 1998.

[35] R. S. Maxwell and B. Balazs. Residual dipolar coupling for the assessment of cross-link density changes in gamma-irradiated silica-pdms composite materials. *Journal of Chemical Physics*, 116(23):10492–10502, 2002.

[36] M. T. Vlaardingerbroek and J. A. Den Boer. *Magnetic Resonance Imaging.* Springer, Berlin, 2 edition, 1999.

[37] P. Glover and Sir P. Mansfield. Limits to magnetic resonance microscopy. *Reports on Progress in Physics*, 65(10):1489–1511, October 2002.